SHEAR BEHAVIOR OF PRE-CRACKED, REINFORCED CONCRETE BEAMS RETROFITTED WITH GLASS FIBER REINFORCED PLASTIC SHEET

by

Wilasa Vichit-Vadakan

B.S. in Civil Engineering, Cornell University, Ithaca, New York
(1995)

Submitted to the Department of Civil and Environmental Engineering in partial fulfillment of the requirements of the degree of

Master of Science in Civil and Environmental Engineering

at the

Massachusetts Institute of Technology

January 1997
[February 1997]

Signature of Author _____
Department of Civil and Environmental Engineering
January 1997

Certified by _____
Oral Buyukozturk
Professor, Departmental of Civil and Environmental Engineering
Thesis Supervisor

Certified by _____
Joseph M. Sussman
Chairman, Departmental Committee on Graduate Studies

SHEAR BEHAVIOR OF PRE-CRACKED, REINFORCED CONCRETE BEAMS RETROFITTED WITH GLASS FIBER REINFORCED PLASTIC SHEET

by Wilasa Vichit-Vadakan

Abstract:

The use of glass fiber reinforced plastic (GFRP) sheets as external reinforcements has been shown to increase the flexural strength of reinforced concrete beam. However, the failure behavior is not yet understood thoroughly. The retrofitted beams have a tendency to fail in a number of different failure modes distinctly different from traditionally reinforced concrete beam; examples of these failure modes include shear failure, concrete crushing, and the failure of the concrete between the internal and external reinforcements. In this research, the experimental and analytical investigations were conducted to study the shear behavior of pre-loaded, steel reinforced concrete beam retrofitted with epoxy bonded GFRP sheet on the tension side of the beam.

In the experimental program, 3 inches x 5 inches x 42 inches (7.6 cm x 13 cm x 107 cm) concrete beams reinforced with two #3 50-ksi (345-GPa) steel rebars were cast and preloaded before the GFRP is applied to the soffit. A 4-point loading scheme was used. The most apparent experimental variable was the length of the GFRP. The beams retrofitted with the 36-inch (91-cm) long GFRP showed all six forms of the failure modes observed. In contrast, the beams retrofitted with the 28-inch (71-cm) long GFRP sheet consistently failed due to the failure of the layer of concrete between the internal and external reinforcements. This particular type of failure indicates the high shear stress concentration at the end of the external reinforcement provided by the GFRP. However, the bond along the interface between the concrete and the GFRP was strong so the failure was shifted to the concrete layer adjacent to the interface.

The analytical model is a one-dimensional analysis of the shear stress distribution along the interface between the concrete and GFRP. The results of the analysis confirmed that the shorter external reinforcements cause much higher shear stress concentrations on the concrete beam. The model also showed that higher stress concentrations occur with stiffer GFRP sheets and that the thickness and shear modulus of the epoxy should be within a given range. Outside of that range, the stress transfer may not be effective or the stress concentration may be too high.

The results of both the experimental and analytical programs showed important parameters affecting the shear behavior of the retrofitted beams. The effects of these parameters, including the length of the GFRP, the stiffness and thickness of the GFRP, the strength of the concrete, and the shear modulus and thickness of the epoxy, should be further studied.

Thesis supervisor: Oral Buyukozturk
Title: Professor, Department of Civil and Environmental Engineering

To my parents,
Dr. Vinyu and Mrs. Chantima Vichit-Vadakan
and
To my mentor and friend, Professor Mary Sansalone,

You were my strength when I was weak...
You were my voice when I couldn't speak...
You were my eyes when I couldn't see...
You saw the best there was in me...
Lifting me up when I couldn't reach...
You gave me faith 'cause you believed...
I'm everything I am because you loved me...

- Words and music by Diane Warren -
- Performed by Celine Dion -

If only there were words for me to express how grateful I am...

Acknowledgements

I would like to begin by thanking Professor Oral Buyukozturk, my thesis advisor, for allowing me to pursue this thesis project. My sincere appreciation goes to Professor Chris Leung for his time and patience in answering my questions, helping me formulate the analytical model, and reviewing parts of my thesis.

I would like to thank Eliza Dubroff, MIT '98, my undergraduate research assistant, for without her willingness to work, curiosity for the subject, and intuition for practicality, this project would never have gotten off the ground, much less completed. She has taught me how important it is to care about and enjoy one's work. More importantly, thank you for your friendship.

My appreciation is extended to all those who helped me with this experimental project. To Dr. Jack Germaine, for his help with acquiring and setting up the displacement transducers and data acquisition system. To Stephen Rudolph, for his constant help with everything that went wrong and right in the labs. To Charlie Caruso, at Barker Steel, for donating all the steel that was used for this project. To Leon Wegner, for his time spent teaching me about the lab and sharing the limited resources of our labs, although his project should have taken much higher precedence. To Tony Simone, for helping with digitizing graphs and the use of some of the testing machines in the lab. To Brian Hearing, who had done some of the preliminary literature survey and helped with acquiring some of the concrete materials.

I would never have pursued a graduate degree in civil engineering if it was not for the enthusiasm shown to me by the faculty at my alma mater, Cornell University, for they have taught me, by example, how to think and care about my work. To Professor Mary Sansalone, who ignited my love and curiosity for structures and horses and continued to advise me about everything in life. Dr. Nicholas J. Carino, at the National Institute of Standards and Technology, also continued to advise me in this research project.

I also want to thank my friends in Boston and others throughout the world who constantly reminded me that I can do it and was always there to hear me complain about a lousy day. To name a few: Danielle Suh, Wipanee Phupakdi, Kanokporn Boonsirichai, Tanita Sirivedhin, my aunt in Chula, Jain Charnnarong, and all my friends at ATSIST. I would also like to thank Drs. Donald and Joan Korb and Cynde and David for checking on my well being and feeding me with home cooked meals on special holidays that I could not be with my family. My thanks go to my friends at Dana Hall Riding Center, especially Kim Summers, for providing

me with a place to retreat to, away from the city, and sharing with me their love of horses, which I will keep with me for the rest of my life.

Within the last few weeks of the completion of my thesis, a few people have stepped in to give me the final boost to the top. This thesis would never have been completed without their help. My sincerest gratitude goes to Cynthia Stewart and Pat Dixon for not giving up hope on my thesis long after mine was buried in the sand.

Lastly, but most importantly, I want to thank my parents and two brothers. I would never have considered pursuing, much less successfully complete, a degree here without all your love and support. You have given me everything that I am today. I thank you and salute you...

Muchisimas gracias!   *Thank you!*   แด้วขอขอบพระคุณทุก ๆ คนค่ะ

Table of contents

List of tables

List of figures

Conversion units

1 inch = 0.0254 meters

1 psi = 6.895 kPa

$1\ in^2$ = 645.2 mm^2

1 lb = 4.448 N

Nomenclature

ACI	American Concrete institute
ASTM	American Society for Testing and Materials
FRP	fiber reinforced plastic
GFRP	glass fiber reinforced plastic
GPa	gigapascals
in	inches
kips	1000 pounds
kN	kilonewtons
kPa	kilopascals
ksi	kips per square inch
lb	pounds
m	meters
mm	millimeters
N	newtons
NDT	nondestructive testing
psi	pounds per square inch

Chapter 1 Introduction

1.1 Problem definition

The deterioration of the aging infrastructure is gaining much public interest. Load demands on structures continue to increase as these structures get older and deteriorate with time. The Federal Highway Administration estimates that over 50% of the bridges in the U.S. are not capable of carrying the load capacities required for today's traffic. Tearing down existing structures and building new ones is not always the most economical or practical solution. Along with nondestructive testing (NDT), the rehabilitation and repair of structures is gaining much interest in the field of structural engineering. Structures need to be retrofitted either to regain their original design strength or to strengthen them further such that they can carry the increasing load demands of today.

Reinforced concrete structural elements can be found everywhere, for example as slabs in steel structures. Problems with reinforced concrete structural elements include deterioration of the concrete, deterioration of the steel, and cracking of the structural element. These problems undermine the strength of the concrete. A number of repair techniques have been developed, including plating (externally bonded plates), doweling (dowels anchoring old and new concrete), and epoxy crack sealants. In many cases, cracking is such a significant problem that epoxy sealants are not effective. The cracks are often located in areas where pouring a new layer of concrete is not an option either. Plating, therefore, has gained popularity as a repair and strengthening technique for reinforced concrete structural elements. Initially, plating involved the use of steel plates as external reinforcements, but corrosion of the external reinforcements have been a significant problem so other materials are being investigated to replace this use of steel.

The field of aeronautics has used fiber reinforced plastics (FRP's) for a number of decades because of their lightweight, high strength, and versatility. Recently, FRP's have been applied to civil structures to replace steel in plating. It offers two very important characteristics. First, it does not corrode so exposure to harsh environments does not

undermine its strength. In addition, FRP's are lightweight. The application of heavy steel plates on to soffits of beams is often troublesome; lighter materials are preferred whenever possible. FRP's can be designed with different mechanical properties by choosing different types of fibers and matrix. They can also be made into very thin sheets, often times as thin as 0.15 mm (5.9 x 10^{-3} inch). Although the use of composite materials in structures points to a promising future, the composite action of the retrofitted beams is still not well understood. This study will further explore failure behavior of this type of composite beams.

1.2 Research objectives

The objective of this study is to investigate the integrity of the composite system consisting of cracked, reinforced concrete beam retrofitted with glass fiber reinforced plastic (GFRP). One particular focus of the study is the shear behavior of the retrofitted composite beam caused by the increase in the flexural strength, from the additional external reinforcement, as it approaches the shear strength. The behavior of the composite system is observed as experimental parameters are varied: the surface texture of the GFRP, the length of the GFRP, and the design shear strength of the reinforced concrete beam. Analytical studies investigate the effects of the following parameters: the Young's modulus of the GFRP, the thickness of the GFRP, the length of the GFRP, the shear modulus of the epoxy, the thickness of the epoxy, and the strength of the concrete on the shear stress distribution along the interface between the concrete and the GFRP. The effects of these variables on the behavior of the retrofitted beams are studied to develop further understanding of this form of composite system.

1.3 Approach

This project will be developed from two approaches. First, the behavior of the retrofitted beams is observed through experimental studies. An analytical model of the beams is then developed to model the effects of different parameters on the behavior of the beams.

1.3.1 Experimental approach

Structures to be retrofitted with external FRP reinforcements are often already damaged. In particular, significant cracking may have already occurred. To better model this,

the beams tested in the experimental program will be pre-loaded to introduce cracks before they are retrofitted with the GFRP sheets. Experimental variables will include the shear strength of the unretrofitted reinforced concrete beams (by varying the spacing of the shear stirrups), the surface texture of the GFRP, and the length of the GFRP. GFRP was chosen for use in this project because it was both readily available and inexpensive. During the loading, the load and displacement at the midspan of the beams will be recorded, to allow load vs. displacement plots to be produced later. Photographs of the beams will also be taken to record the different failure modes. In the end, trends will be drawn from these results to determine dominant failure modes and identify their possible causes.

1.3.2 Analytical approach

The effects of other parameters were studied in the analytical program: the Young's modulus of the GFRP, the thickness of the GFRP, the length of the GFRP, the shear modulus of the epoxy, the thickness of the epoxy, and the strength of the concrete. The analytical program is designed to gain a better understanding of the effects of these parameters on the shear stress distribution along the interface between the concrete and the GFRP. Such an understanding is critical for the development of an effective retrofit method. Past studies have shown two primary failure modes: the delamination of the GFRP and the failure of the concrete layer between the internal and external reinforcements. Both of these failure modes are likely affected by the shear stresses along the interface between the GFRP and the concrete. A one-dimensional analysis of the shear stress distribution along the interface will be performed.

1.4 Organization

The literature survey is presented in Chapter 2. This chapter presents available repair techniques for reinforced concrete structural elements, available types of FRP's, and past research on GFRP's as external reinforcements. Chapter 3 presents the experimental program. The scope is first presented in detail, including calculations for the beam design, the experimental parameters, and the experimental schedule. Then, the materials are presented and discussed. Finally, the experimental methods and equipment are presented. The following chapter, Chapter 4, discusses the results from the experiment. Trends, expected and unexpected, are described from quantitative data of the experiments, and the qualitative

findings are provided. The analytical approach for this project is presented in Chapter 5. The shear stress distribution between the concrete and the GFRP is analyzed with variations of different parameters. Finally, Chapter 6 provides a summary, conclusions, and recommendations for future work.

Chapter 2 Literature survey

2.1 Structural deterioration in reinforced concrete structures

Structural deterioration of reinforced concrete structures can occur in many different forms. Deterioration of the material is a significant problem. Corrosion can greatly undermine the strength of reinforced concrete members. Not only does corrosion destroy the integrity of the steel, corroded steel expands, forcing the surrounding concrete to crack or even popout. Concrete deterioration can be shown by cracking, scaling (flaking away of the surface mortar), honeycombing and air pockets, or extreme wear through physical or chemical means (Xanthakos 1996). On a larger scale, cracking can occur when structural members and joints are overloaded or loaded along a weaker axis. In all cases, the strength of the reinforced concrete structural member decreases significantly and must be restored.

Detection of unsound concrete and reinforced concrete members can be done in a number of ways. Visual inspection is often the first option as it can pinpoint significant problems with little cost. Visual inspection of inaccessible areas can be done by drilling holes for inspection purposes. Often times, the material properties of the concrete can be evaluated through corings. More recently NDT methods have allowed the evaluation of possible problems within the concrete without permanently disturbing the concrete. Problems such as corrosion of steel reinforcing bars, honeycombing, alkali-aggregate reaction, and sulphate attack of the concrete can be detected without drilling.

As these problems are detected, the structure must be repaired. Often times, restrictions on the repair techniques are dependent upon the use of the structure. For example, closure of interstate highway bridges or its underpass can cause significant havoc and should be avoided. The next section explores repair techniques commonly used today.

2.2 Traditional repair techniques for reinforced concrete

Repair techniques for problems in reinforced concrete structures vary, depending on the size and location of the problem. Simple repair techniques can involve the application of mortars to fix small cracks or small amounts of spalling. More complicated problems, like strengthening of the structure, can be solved using a method called plating, the application of steel plates as external reinforcements. Structures that need more deflection control and higher amounts of strengthening may need to be post-tensioned.

Small amounts of cracking, especially those that do not undermine the strength of the structural member but need to be fixed to prevent corrosion of the steel, can be fixed by applying epoxy crack sealants or different types of mortar. Materials often used for these applications include cement based mortar, quick-setting non-shrink mortar, epoxy mortars, resin-based polymer concrete, and cement-based polymer concrete. If the problem is significant enough to require new concrete to be poured and the location allows such a repair method, dowels can be used to hold the new and old concrete together. The surface preparation often requires careful planning and preparation to achieve good bond. In many cases, this type of repair method is often sufficient for the life of the structure, if done carefully.

More complicated problems can be solved through plating, the addition of external steel plates as reinforcements to increase the section modulus and load capacity of the structural member. Although this method has been successful in the past, there are some significant problems. Without a layer of concrete cover, the steel can corrode in harsh environments, making the repair ineffective within a very short time period. In addition, the application of epoxy-bonded steel plates often requires scaffolding to be built because the steel plates are heavy. However, these problems may be solved with the use of FRP sheets that have similar strengths but are much lighter and can be manufactured to withstand harsh environments. This method will be the topic of this study.

Finally, if significant deflection control or strengthening is needed, post-tensioning of the structure maybe required. This can be done in a number of ways: one is very similar to plating. In this case, external plates are placed in tension before being applied to the structural member, inducing a pre-stressing force on the member. However, this method remains experimental due to problems with anchorage and needs to be further investigated. The design of post-tensioning repair work requires both skill and experience in working with pre-stressed concrete structures.

2.3 Materials for external reinforcements

The FRP has two primary components: the fibers and the matrix. The matrix is dependent upon the type of fiber used. The three primary materials used for fibers are glass (GFRP), carbon (CFRP), and kevlar or aramid (KFRP). Table 2.1 shows a comparison of the Young's modulus (E), the strength (σ_f), and relative cost per unit volume. All of these materials have been tested as external reinforcements. In particular, a group at the University of Delaware has experimented with the use of KFRP and GFRP (Chajes et al 1994, Chajes et al 1995), including some durability tests. Because KFRP was much more expensive than GFRP, the group found that the results did not prove to be significant enough to warrant the use of the much more expensive KFRP. Pioneering work on the use of CFRP, especially as external reinforcements, has been done in Switzerland (Deuring 1993, Meier 1991, Meier 1993, Meier et al 1992). The materials were produced by the Swiss Federal Laboratories themselves and have been applied to a number of structures that are in use, including bridges and buildings (Duering 1993, Meier 1993, Meier et al 1992). However, CFRP's have not gained much interest in the U.S. because they are expensive and not as readily available as GFRP's.

In the U.S., GFRP's are more readily available and relatively inexpensive. From the table, note that the relative cost per volume cost of CFRP's and KFRP's are an order of magnitude higher than that of GFRP's. Some argue that the additional strength and stiffness offered by CFRP's and KFRP's are significant advantages and warrant their use. However, the analytical chapter will show that the gain in stiffness may seriously undermine the strength of the retrofit technique. In addition, one of the objectives of the study is to observe the shear behavior of the beam because of the stress concentration. High stress concentrations at the ends of the external reinforcement are the likely cause of significant delaminations. Materials with very high ultimate strength may not be used to its full potential either because the composite strength of the retrofitted beam may be governed by the shear strength of the beam instead of the flexural strength. This is because the beams are retrofitted in shear and not flexure. Therefore, GFRP was chosen for this study for practical reasons: more economical and available.

2.4 GFRP's as external reinforcements

GFRP sheets have been used as external reinforcements for concrete structures because, as mentioned above, it is both readily available and relatively inexpensive, in comparison to other FRP's. Many types of GFRP sheets have been introduced for use as external reinforcements. Many research groups have focused on the use of GFRP as external reinforcements for concrete structures, as will be discussed in the following sections. These sections will further explore the different types of GFRP sheets and past research within this field.

2.4.1 Types of GFRP reinforcements

A number of different forms of FRP's with potential use as external reinforcements have been introduced. One type is called a fabric. The fibers are woven into a fabric, like a net. When placed onto a concrete structure, the epoxy serves two purposes: as a bonding agent and as the matrix. Another type of FRP, applied similarly to fabrics, is called tow sheet. In this form, the fibers are lined up in one direction and temporarily laminated onto paper. Again, the epoxy acts as both the bonding agent and the matrix. The paper backing is removed immediately after application. Finally, the last type of composite is a direct extension of steel used in plating. Plates or sheets of the FRP are applied to the concrete surface with epoxy as the bonding agent.

Fabrics

A fabric, as mentioned above, is made of interwoven fibers. As external reinforcements, a layer of epoxy is applied to the concrete surface. Then, the fabric is applied, and another layer of epoxy is applied on top of that. The epoxy acts as both the matrix for the composite and the bonding agent between the FRP and the concrete. Strengths of these composites vary significantly, as with other types of composites.

There are some advantages to using the fabric. The fibers in the fabric are bi-directional and can take tension in both directions. Since they carry no flexural stiffness, the material and the epoxy can conform to any rough surface. This can alleviate problems with providing a strong interfacial bond. However, questions remain on its long-term durability.

Matching the fabric with the proper epoxy will become the most important task since the epoxy acts as both the matrix and the bonding agent.

Tow sheets

Applied in a similar manner as the fabrics, tow sheets have been commonly used in Japan (Chajes 1996). The materials are produced by two Japanese companies: Mitsubishi and Tonen. Fibers are lined in one direction (Tonen 1996). To hold them together, a sheet of paper and a light set of criss-cross fibers are used as a backing to hold the fibers together. The tow sheets have thicknesses ranging from 0.110 to 0.165 mm (4.33×10^{-3} to 6.50×10^{-3} inch). The published strength for glass fibers is 220 ksi (1.53 GPa). In applying the composite, a layer of epoxy is applied first. Then, the tow sheets are applied, and the paper backing is peeled off. Finally, another layer of the epoxy is applied. All of this must take place within the pot life of the epoxy. Again, the epoxy acts as both the matrix and the bonding agent for the glass fibers.

Tow sheets are unidirectional. However, since they are so thin, multiple layers can be oriented in different directions to yield multidirectional strength. Like fabrics, the tow sheets can easily be made to conform to the given surface because it has no flexural stiffness. In addition, if a delamination or void is discovered, epoxy can easily be injected to fill in the void. Since the epoxy acts as both the bonding agent and the matrix, this does not create stress concentrations or undermine the strength in any way. Problems with this form of composite are similar to those of the fabric. The choice of epoxy becomes very important for strength and durability purposes. With more studies into the mechanical behavior and properties of the tow sheets and their durability, the possibilities for its use can make a significant impact on the repair of concrete structures.

Sheets and plates

GFRP sheets and plates are composed of glass fibers embedded in different types of plastic matrix. They are produced through either poltrusion or injection molding. In poltrusion, the fibers are stretched out and pulled through a molten form of the matrix material. Then, it is heated and pressed into its final form. Injection molding is a similar process. Both processes

allow the FRP to be produced in any shape and size. Some materials have limits on minimum thickness or structural configuration, depending on the matrix and the fibers.

GFRP sheets can be applied to the structural member with epoxy as the bonding agent. In some instances, external pressure has been used to ensure stronger bond. Because the sheets are light, heavy scaffolding and equipment is not required. Undoubtedly, the increase in strength of the retrofitted beam is significant. However, the primary problem with this repair method is the behavior of the retrofitted beams. Without a good understanding of the behavior of the retrofitted beams, the strength cannot be predicted with good accuracy.

2.4.2 Results from previous studies

The application of GFRP's as external reinforcements on reinforced concrete structures have been studied by many groups throughout the world. In all cases, the conclusion was that the gain in strength was significant (Arduini et al 1994, Chajes et al 1994, Chajes et al 1995, Deuring 1993, Finch et al 1994, Meier 1991, Meier et al 1992, Ritchie et al 1991, Roberts 1989, Roberts and Haji-Kazemi 1989, Saadatmanesh and Ehsani 1990, Saadatmanesh and Ehsani 1991, Schwegler 1994, Sharif et al 1991, Sierakowski et al 1994, Triantafillou et al 1992, Zariba et al 1994). Some groups have attempted to build models to predict the strength of the beam, but they all have assumed flexural failure of the retrofitted beams (Chajes et al 1994, Sierakowski et al 1994, Triantafillou et al 1992, Zariba et al 1994). Other types of failure have been observed, especially those resulting from problems with the shear strength of the beam and the shear transfer between the concrete and the GFRP (Ritchie et al 1991, Saadatmanesh and Ehsani 1990, Saadatmanesh and Ehsani 1991, Sharif et al 1991). Past research has shown promising trends, especially those in strength gains, but they also brought up questions that need further investigation to improve the understanding of the behavior of reinforced concrete beams retrofitted with externally bonded GFRP.

Using GFRP as external reinforcements for strengthening existing reinforced concrete structure has shown to be effective, both in research and on applications to real structures. Reported strengths of the beams have been as much as 200% of the controlled beam (Saadatmanesh and Ehsani 1990). However, in some cases, to prevent the beams from failing prematurely, the beams had to be reinforced in shear, often by the use of C-clamps (Ritchie et al 1991). Reported strength gains must be read with care, noting the initial beam design and precautions taken to assure a flexural failure.

Although most experimental studies have focused on the strength gain of the application of external reinforcements, that is not necessarily the only potential for its use. GFRP's as external reinforcements have been used for crack control (Chajes 1996, Finch et al 1994). One particular case, because there was not enough transverse reinforcements for the box beams, cracks formed along the length of the beam. Although the strength of the bridge was not in jeopardy, cracking allowed the penetration of water and salt to corrode the steel. To fix the problem, GFRP tow sheets were applied transverse to the length of the beam. It was determined that the application of the tow sheets would not affect the flexural longitudinal strength of the beam. Therefore, the retrofit would only affect the problem in question. Two years after the application of the tow sheets, the cracking problem has not resurfaced.

Models predicting the strength of beams have also been proposed. In most cases, these models assume flexural failure of the beams. Simple models assuming that plane sections remain plane throughout the retrofitted beams have been tried, and the corresponding experimental result yielded strengths within ±5% of the analytical result (Chajes et al 1994). However, it should be noted that the prediction of the strains in the FRP was not as close, probably because the model assumed that concrete did not take tension. Two other groups modeled unreinforced concrete beams retrofitted with the FRP plates (Triantafillou et al 1992, Sierakowski et al 1994). These models were neither simple nor practical in terms of applying to reinforced concrete structures. Finally, a group attempted to present guidelines for the design of this retrofit method (Ziraba et al 1994). In this case, a finite elements model was developed, and an experimental program was done to confirm the results. The results yielded significant inconsistencies. The theoretical model yielded good results when the steel yielded at failure. However, when there was interface failure, the theoretical model over-predicted the strength by 16% to 70%. These models have highlighted the difficulty in producing an analytical model for the application of FRP's as external reinforcements for reinforced concrete. Significant variations in the FRP properties, bond integrity, damage in the existing beam, and the ultimate failure mode of the retrofitted beam play important roles in the failure of the retrofitted beams. In all cases, the beams were modeled from sound beams, without any pre-existing cracks or other types of faults.

Part of the problem with not being able to produce a more accurate model is the failure mode of the beams. The retrofitted beams can fail in a number of ways: shear failure because the shear strength is lower than the flexural strength, failure of the interface between the concrete and the FRP, and the failure of the concrete layer between the FRP and the steel, to

name a few. As the flexural strength of the beam is increased to approach the initially designed shear strength of the beam, the beam tends to fail in shear, causing a brittle failure. One likely solution is the use of jackets as external shear reinforcements also, thus increasing the shear strength along with the flexural strength. Another form of failure is the interface failure due to high shear stresses along the interface between the concrete and the external reinforcement. This problem can be solved by matching the mechanical properties of the epoxy with those of the concrete and FRP better and developing better technique to improve the quality of the bond. Finally the failure of the concrete layer between the FRP and the steel, causing a premature failure of the retrofitted beam, is a significant problem reported by a number of research teams (Ritchie et al 1991, Saadatmanesh and Ehsani 1990, Saadatmanesh and Ehsani 1991, Sharif et al 1991). This problem has yet to be understood well. It is likely due to the shear stress concentration at the ends of the external reinforcement. This type of failure mostly occurs when the composite does not extend all the way to the support, thus ending within the high shear region of the beam. Further studies need to be done to determine ways of alleviating the stress concentration or define critical locations so that the shear stress can be minimized.

Although these studies have confirmed a number of trends, like the gain in strength, they have also proposed a number of possible problems, like the different failure modes. Questions remain as to how to predict the failure mode of the retrofitted beams and, consequently, predict the strength of the retrofitted beams. Unless that can be done with consistency, the application of GFRP's as external reinforcements to retrofit existing reinforced concrete structures cannot be done efficiently. To be able to do this, better understanding of the failure mode of the retrofitted beams is needed.

2.5 Ties to research objectives and approach

The literature survey has brought up many questions. Two primary problems will be further investigated in this study. The failure mode of the retrofitted beams, especially as the flexural strength is increased to approach the design shear strength of the beam, will be investigated in the experimental program. The stress concentration at the ends of the external reinforcement, causing the failure of the concrete layer between the FRP and the internal reinforcing steel, will be studied in the analytical program. The focus of this project is towards observing the behavior of damaged beams that are retrofitted. To do this, the beams will be

pre-loaded to introduce initial shear and flexural cracks before they are retrofitted with epoxy bonded GFRP sheets. Experimental variables will include variations in the shear strength of the beam, the surface treatment of the GFRP, and the length of the GFRP sheet. An analytical model will also be developed to study the effects of different parameters on the shear stress distribution along the interface. Material parameters of interest include the Young's modulus of the GFRP, the shear modulus of the epoxy, and the strength of the concrete. Physical parameters to be varied include the length of the GFRP sheet, the thickness of the GFRP sheet, and the thickness of the epoxy. The results obtained from these studies will provide further behavioral knowledge contributing to the future development of this method as a viable retrofit technique.

Table 2.1 Comparing modulus, strength, and cost of FRP's (Ashby and Jones 1980)

Material	Young's modulus (E) (GPa)	Strength (σ_f) (MPa)	Relative cost per unit volume (Mg/m^3)
Glass fiber reinforced plastic (GFRP)	30	400	30
Kevlar fiber reinforced plastic (KFRP)	70	350	200
Carbon fiber reinforced plastic (CFRP)	150	1000	500

Chapter 3 Experimental Program

This chapter provides information about the experimental scope, materials used (concrete materials, steel, GFRP), preparation methods, and testing apparatus and methods.

3.1 Experimental scope

Often times, beams that need retrofitting will be damaged beams, or at least beams with some cracks in them. To better understand the behavior of retrofitted beams, the beams in this experiment will be preloaded to introduce both flexural and shear cracks along the span of the beam. These reinforced concrete beams will be designed and built with both shear and flexural steel reinforcements. They will be loaded under 4-point bending. After the initial loading, the beams will be unloaded and the GFRP applied. Finally, the beams will be loaded to failure. Load and displacement at the midpoint of the beam will be measured and stored using a data acquisition system during all loadings.

3.1.1 Test specimens

This section describes the design process for the beams. The reinforced concrete beams were initially designed according to ACI Code, with calculations for the flexural and shear strength. Then, the design calculations were extended to predict the strength of the composite beam after the GFRP is applied. Some simplifying assumptions were used for these calculations. The following sections include descriptive summaries of the design calculations.

Beam design

Due to the limitations of the testing machines, the distance between the supports of the beam was limited to 36 inches (91 cm). Therefore, the cross-section of the beam was

designed to be 3 inches x 5 inches (7.6 cm x 13 cm) to avoid deep beam behavior. A deep beam is defined as beams having a ratio of unsupported length to depth of beam of 5 or less, or the shear span to the depth ratio of less than 2 (Nilson and Winter 1991). In this experiment, the ratio of unsupported length to depth of beam is 7.2, and the shear span to depth ratio is 2.4.

The beams were cast with the dimensions 3 inches x 5 inches x 42 inches (7.6 cm x 13 cm x 107 cm). Two No. 3 50-ksi (345-GPa) steel reinforcing bars were used as flexural reinforcements. Shear reinforcements were made of 36-ksi (248-GPa) ¼ inch (0.64 cm) diameter pencil rods bent into rectangular stirrups. The beam design was made according to ACI 318-95 with the following dimensions and properties for calculations:

Concrete strength	$f_c =$	5.0	ksi	34.5	GPa
Yield strength of the flexural steel	$F_y =$	50	ksi	345	GPa
Yield strength of shear stirrup	$F_v =$	36	ksi	248	GPa
Area of flexural steel	$A_s =$	0.22	in^2	1.42	cm^2
Area of shear stirrup	$A_v =$	0.098	in^2	0.633	cm^2
Width of beam	$b =$	3	in	7.6	cm
Distance from top of beam to flexural steel	$d =$	3.5	in	8.9	cm
Height of beam	$h =$	5	in	13	cm

From the equilibrium of forces at any cross-section of the beam:

$$0.85 f'_c\, ab = F_y A_s.$$ Equation 3.1

Using the properties from above,

$$a = 0.863 in.$$

Therefore, the nominal moment is:

$$\phi M_n = 0.9 F_y A_s (d - \frac{a}{2}) = 30.4 kip - in$$ Equation 3.2

Since the beams were tested in 4-point bending and supported at 36 inches (91 cm), the expected failure load of the beams was calculated to be 5.06 kips (22.5 kN). This flexural design strength was kept for all beams.

The shear strength of the beam can be calculated as follows:

$$V_c = 2\sqrt{f'_c}\, bd = 1484 lbs$$ Equation 3.3

$$\phi V_n = 0.85(V_c + \frac{A_v F_v d}{s})$$ Equation 3.4

Two stirrup spacings were required as part of the experimental variables: 5-inch (13-cm) and 7-inch (18-cm). From Equation 3.4, the expected shear strengths of the beams with 5-inch (13-cm) and 7-inch (18-cm) stirrup spacings are calculated to be 6.72 kips (29.9 kN) and 5.53 kips (24.6 kN), respectively.

From the above calculations, the unretrofitted beams should fail in flexure when the load reaches 5.06 kips (22.5 kN) without any external reinforcements. However, when the GFRP is added onto the beam, the flexural capacity should increase such that the shear capacity will govern in some beams. Figure 3.1 shows the schematic view of the beam design.

Expected strength of retrofitted beams

With the addition of the external GFRP reinforcement, the flexural strength of the beam is expected to increase significantly. The following assumptions and simplifications will be made during the calculation of the new strength of the beam:

1. plane sections remain plane;
2. the steel has fully yielded;
3. the concrete is just about to crush, similar to ACI beam analysis;
4. the GFRP behavior is linearly elastic.

Although the fourth simplification is assumed, it will be shown later that the assumption is not always valid. The Young's modulus of the GFRP, used in this calculation, is the calculated average of the initial tangent modulus of five tension specimens. More details about the tensile tests of the composite can be found in section 3.2.1. In addition to the mechanical properties introduced above, the following properties will be used in the calculation:

Young's modulus of the GFRP	$E_p =$	494	ksi	3.41 GPa
Young's modulus of the steel	$E_s =$	29000	ksi	200 GPa
Maximum strain in the concrete	$\varepsilon_c =$	0.003		

Other variables used include:

F_p = stress in the GFRP;

t = thickness of GFRP;

b' = width of the GFRP;

ε_p = strain in the GFRP;

a = height of the concrete effective in compression.

From Figure 3.2, the following equilibrium and compatibility equations were used in the calculation to find the stress in the GFRP:

$$0.85 f'_c ab = F_y A_s + \sigma_x b' ;$$

Equation 3.5

$$\frac{\varepsilon_c}{a} = \frac{\varepsilon_p}{h-a} = \frac{\sigma_x / E_p}{h-a} .$$

Equation 3.6

In this experiment, the width of the GFRP is made to be the same as the width of the beam so:

$$b' = b .$$

From Equations 3.5 and 3.6, the following were calculated:

$$\sigma_x = 6.543 kips$$
$$a = 0.9234 inch$$

Then, the nominal moment is calculated by:

$$\phi M_n = 0.9 \left[A_s F_y (d - \frac{a}{2}) + \sigma_x bt(h - \frac{a}{2}) \right] = 33.2 kip - in .$$

Equation 3.7

Since the beams were tested in 4-point bending, the expected failure load is calculated to be 5.53 kips (24.6 kN). Because there was no shear strengthening, only the flexural strength is increased by the addition of the external reinforcement. Note that this new flexural strength approaches the design shear strength of the beams with 5-inch (13-cm) and 7-inch (18-cm) stirrup spacings, at 6.72 kips (46.4 kN) and 5.53 kips (24.6 kN), respectively. This was done to observe the shear behavior of the retrofitted beams.

3.1.2 Experimental schedule

The preparation and testing of each set of four specimens followed a nine-day schedule. The schedule allowed some overlapping such that two sets can be worked on at any one time. The following is the schedule:

Day 1 Preparations

     Sift cement and aggregates. Bend #3 bars to make 180° hooks. Make stirrups.

Day 2 Mix

     Mix concrete and cast into beams and cylinders.

Day 3 Strip and place in curing tank

     Strip molds. Place beams and cylinders in lime water curing tank.

Day 4 Cure

Day 5 Flip

> Turned beams over to make sure that all surfaces were allowed to be exposed to the lime water.

Day 6 Cure

Day 7 Cure

Day 8 Pre-crack and epoxy

> Remove all beams and cylinders from the curing tank. Weigh beams. Load all beams to an initial midspan displacement of 0.15 inch (0.38 cm). The unretrofitted beams were left in the laboratory overnight. Otherwise the GFRP was epoxied on to the beams after pre-cracking.

Day 9 Fail

> Test all beams to failure.

3.1.3 Experimental parameters

Three variables will be used in the experiment: stirrup spacing, surface texture of the GFRP, and length of the GFRP. Table 3.1 shows how the parameters applied to the 32 beams tested in this experiment.

From preliminary tests, two stirrup spacings, 5-inch (13-cm) and 7-inch (18-cm), were chosen for the project. The two different stirrup spacings will be used to control the crack size and the shear strength of the beam. As mentioned in section 3.1.1, the beams were designed for shear strengths of 6.72 kips (29.9 kN) for the 5-inch (13-cm) stirrup spacing and 5.53 kips (24.6 kN) for the 7-inch (18-cm) stirrup spacing. Although the beams were initially over-designed in shear, the addition of the GFRP will increase the flexural strength to approach that of the shear strength of the beam. However, the GFRP would not affect the shear strength of the beam. This will allow the study of the propagation of shear cracks and any interaction between the shear cracks and the laminate interface.

The surface texture of the GFRP, as will be explained in the section describing the GFRP, is another variable. This will be done to test possible variations in the strength of the bond as will be indicated by delaminations. The rougher surface of the GFRP is expected to allow a stronger GFRP-epoxy-concrete bond. In addition, the bond strength is expected to have less variation. The bond strength with the smoother surface can be as strong as the roughened surface, but that requires a higher level of quality control in working with the epoxy

and the application of the GFRP. The bond strength will be critical when the shear crack propagates all the way to the tension face of the beam.

The length of the GFRP is the third variable. The length of the GFRP was varied to study possible changes in the failure more of the beams. A number of research groups have mentioned the failure of the concrete layer between the internal and external reinforcements (Ritchie et al 1991, Saadatmanesh and Ehsani 1990, Saadatmanesh and Ehsani 1991, Sharif 1991). It is hypothesized that this mode of failure is affected by the location of the end of the external reinforcement with respect to the shear span. To confirm this, two different external reinforcement lengths will be studied. The first GFRP length to be tested will be the full unsupported length of the beam, 36-inches (91-cm). Note that the supports will not interact with the GFRP. The second GFRP length is 28-inches (71-cm). The shorter GFRP length will extend 7 inches (18 cm) into the high shear area on both sides of the beam. As mentioned in the Literature Survey, other research groups have observed that a higher incidence of the failure of the concrete layer between the GFRP and the steel when the GFRP did not extend all the way to the support. The shorter length was designed to extend approximately half way into the high shear area. In addition, the pre-load cracks were noted, and it was decided that the 28-inch (71-cm) length of the GFRP is sufficient to extend beyond all initial cracks.

The beams were designated according to stirrup spacing – length of GFRP – surface of GFRP. The stirrup spacings were designated by S5 for 5-in (13-cm) spacing and S7 for 7-in (18-cm) spacing. The lengths of the GFRP were designated by 28 for 28-in (71-cm) long and 36 for 36-inch (91-cm) long. The surface textures were designated by SM for smooth and RO for roughened GFRP. For example, S5-28-RO means a beam with 5-in (13-cm) stirrup spacing and 28-in (71-cm) long roughened GFRP. Note that the beams without external reinforcements were only designated by their stirrup spacings.

3.2 Materials

3.2.1 Materials and preparation

This project involved the use of four materials: concrete, steel, GFRP, and epoxy. This section describes the materials used.

Concrete

Type III cement, pea gravel, and mortar sand were bought from Waldo Brothers in South Boston. Type III cement, sold under the brand name, Dragon, came in 94 lbs (42.6 kg) bags. The cement was sifted using a No. 14 sieve and kept in an air-tight plastic container until mixing time. The cement was sifted to remove any lumps that can end up forming weak spots in the final specimen. The pea gravel came in 80 lb. (36.3 kg) bags and was sifted using No. 10 sieve. Any material that went through the sieve was considered too fine and discarded. The maximum aggregate size for the pea gravel was ½ inch (1.27 cm). Sand came in 70 lbs. (31.8 kg) bags. Again, the No. 10 sieve was used, and materials considered too coarse were discarded. The aggregates were stored in separate plastic containers until mixing time. Cold water from the tap was used for mixing. The mix proportion for the concrete is shown on Table 3.2. The water-cement ratio (w/c) was 0.55. The high w/c was needed to give enough workability while two people cast and compact all four beams and cylinders because superplasticizers were not used in this experiment. The weight ratio of cement:fine aggregate:coarse aggregate was 1:4.5:1.6.

Reinforcing Steel

Steel was acquired from Barker Steel in Watertown, MA. The longitudinal bars were #3 50-ksi (345-MPa) epoxy coated deformed bars. They were cut to 52 inches (1.37 m) in length. 180° hooks were manually introduced to the ends of the bars for sufficient development length in the beams.

The stirrups were made from 36-ksi (248 MPa) ¼ inch (6.35 mm) diameter pencil rods. They were cut to 12 inches (0.30 m) in length and bent into the desired form using a hammer. The stirrups were rectangular in shape and had the dimensions of 3.5 inches x 2 inches (8.9 cm x 5.0 cm). Figure 3.3 shows the stirrups and longitudinal bars.

The stirrups and the longitudinal bars were then tied into a steel cage using thin wires. Only the anchoring stirrups were tied to the longitudinal bars. Marks were made on the longitudinal bars as to the locations of the other stirrups, which were placed in the correct locations at the time of casting. Figure 3.4 shows a picture of the stirrups, the longitudinal bars, and the steel cage before casting.

Glass fiber reinforced plastic (GFRP) was chosen for this project because it is readily available and relatively inexpensive. GFRP was bought from Patriot Plastics in Woburn, MA. The raw product was manufactured by Herb Celanese in New Jersey and poltruded by Penn Fiber in Pennsylvania. The tradename of the GFRP is Celanese Nylon Glass Fiber Reinforced Plastic Grade 1600. The GFRP came in black with some gray streaks and shiny luster. The material came in 0.0394 inch (1 mm) thick, 15 inch (0.381 m) wide, and 40 feet long (12.2 m) sheet. The total cost was $188, averaging $3.76/ft^2 ($40/m^2).

The technical specifications of this material indicated that the tensile strength is typically 28,000 psi (193 MPa), and the elongation at break is, typically, 2-4%, when tested according to ASTM D638. However, tensile tests, according ASTM D638 - 95, included as part of the experimental program, indicated a much lower strength for the GFRP. Table 3.3 shows the results from these tests. The average strength was calculated to be 15,700 psi (108 MPa), and the average percent elongation at the maximum load was 5.5%. The measured strength of the GFRP was significant lower than the material specifications provided by the distributor (Herb Celanese 1996). Figure 3.5 shows a typical stress-strain diagram of the test specimens. Note that the behavior is highly non-linear, with decreasing slope in the graph. The decreasing slope, as shown to be the behavior in these materials, may indicate the behavior of short fibers in the matrix. One possible explanation for this problem can be that the fibers were not aligned straight when the GFRP was poltruded, causing some fibers to take on more load and break earlier. The inconsistencies in the published and tested strength of the FRP's should caution their use in design without strict quality control procedures.

In testing the beams, one of the variables used was the surface treatment of the GFRP. Aluminum oxide abrasive 60-grit sand paper was used to roughen up the surface of the GFRP until the shiny luster is removed. An air jet was used to remove any particles left on the roughened surface. This variable was included in the experiment to investigate whether or not the bond strength of the GFRP-epoxy-concrete would be affected. In particular, the roughened surface was expected to behave with more consistency and higher strength.

Epoxy

Sikadur 31, 2-part epoxy was chosen for the use of this project. It is advertised as a high-modulus, high-strength, structural, epoxy paste adhesive. The material specifications indicated properties at 14 days are as follows (Sika Corp 1996):

Tensile strength = 3600 psi (25 MPa)

Elongation at break = 0.4%

Modulus of elasticity = 7.5 x 10^5 psi (52 GPa)

Shear strength = 3400 psi (23 MPa)

The epoxy was mixed using a mixing blade attached to a drill. The drill was run at a low speed for 1 minute of mix time. The sides of the containers were scraped with a plastic paddle for more even mixing. The epoxy was applied on the concrete beam using trowels, and the GFRP sheet was placed onto the beam. For curing, the beams were flipped over onto wax paper such that the weight of the beams was used to provide the constant uniform load for good bond and were left to cure in the lab for 24 hours. The epoxy, when cured, is gray and can easily be camouflaged with the concrete in both color and texture.

3.2.2 Mixing, casting, and curing method

The concrete materials were batched and added into the mixer with water first, followed by coarse aggregate, cement, and fine aggregate, respectively. From the time that the cement was added, the concrete was mixed for 8 minutes. The mixing machine was a mixer of the tilting, open top, revolving blade type with a 2 ft^3 (0.0566 m^3) capacity. The beams were poured in three layers into plywood molds. The first layer of concrete was placed in the mold and was rodded. Then, the steel cage was placed into the mold such that the first layer of concrete will hold the cage in place. A second layer of concrete was then added and rodded. The last layer of concrete was added to fill the rest of the beam and rodded again. When all four beams were completed, two beams at a time were externally vibrated on a vibrating table for 2 minutes each. The cylinders were also vibrated for 2 minutes along with the beams. The beams and cylinders were cured overnight with wet paper towels and plastic wrap on all exposed surfaces. The molds were stripped the following day, and the beams and cylinders were placed in the lime water curing tank until they were ready to be tested.

3.3 Testing apparatus and method

The specimens were tested using a 60-kip Baldwin machine. Figure 3.6 shows a picture of the testing machine. The testing machine is hydraulic, open-loop with manual controls. The beams were tested on medium range, allowing loads up to 24,000 lbs (107 kN). The cylinders were tested using the same machine on high range, allowing loads up to 60,000 lbs (267 kN).

Displacement was measured using a linear variable differential transducer (LVDT). Specifically, the tranducer is a Trans-Tek 0243-0000 D-94. The voltage range is ± 3 volts. It is capable of measuring up to 3 inches in displacement. Displacement was correlated to the change in voltage caused by the movement of the metal core. The transducer was calibrated prior to the beginning of the experiments. Figure 3.7 shows the experimental set-up of the beam in the testing machine with the transducer in place, ready to be tested.

During the tests, both the displacement at mid-span of the beam and the load were measured and recorded every second. The data acquisition system composed of an HP 3497A data acquisition system and a 486 computer. For the final three sets of beams, which included all the beams having GFRP length of 28 inches (71cm), a plotter was used for data acquisition due to the failure of the HP 3497A.

The beams were loaded twice. They were initially loaded, or pre-cracked, such that the center displacement of 0.15 inches (0.381 cm) was achieved. According to the ACI guidelines for allowable midspan deflections:

$$\text{maximum midspan deflection} = \frac{l}{240} \qquad \text{Equation 3.8}$$

$$\frac{36in}{240} = 0.15in$$

The beam was held at that displacement, and a marker was used to draw along the cracks. Figure 3.8 shows a pre-cracked specimen with the drawn cracks. The beam was then unloaded. Whether or not the laminate is applied, the beams were left in the testing lab overnight and tested to failure 24 hours later.

Table 3.1 Testing parameters

Designation	Beam numbers	Stirrup spacing	Plastic length	Plastic surface
S5	3, 4, 7, 8	5	-	-
S7	1, 2, 5, 6	7	-	-
S5-36-SM	17, 22, 26	5	36	Smooth
S7-36-SM	20, 21, 28	7	36	Smooth
S5-36-RO	18, 23, 25	5	36	Rough
S7-36-RO	19, 24, 27	7	36	Rough
S5-28-SM	36, 39, 43	5	28	Smooth
S7-28-SM	33, 37, 42	7	28	Smooth
S5-28-RO	35, 40, 44	5	28	Rough
S7-28-RO	34, 38, 41	7	28	Rough

Table 3.2 Mix proportions

water	25 lbs. 14 oz.	11.7 kg
cement	47 lbs.	21.3 kg
sand	95 lbs. 11 oz.	95.7 kg
gravel	75 lbs. 3 oz.	34.1 kg

Table 3.3 Tensile test results for the GFRP

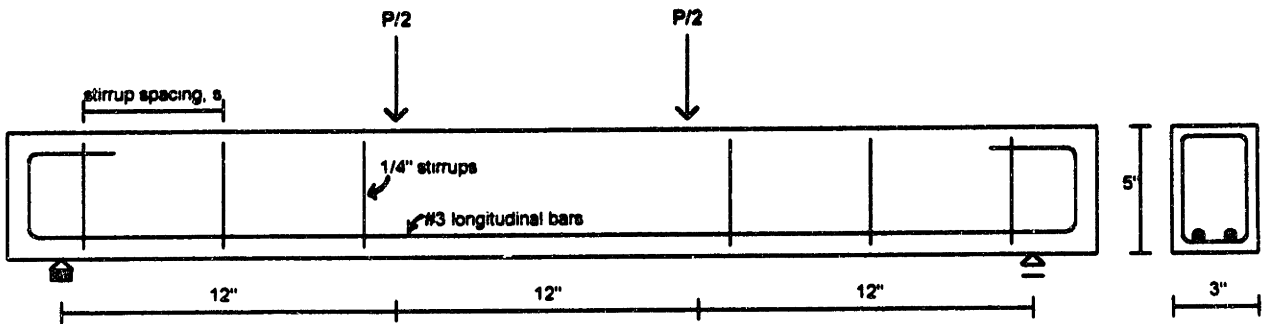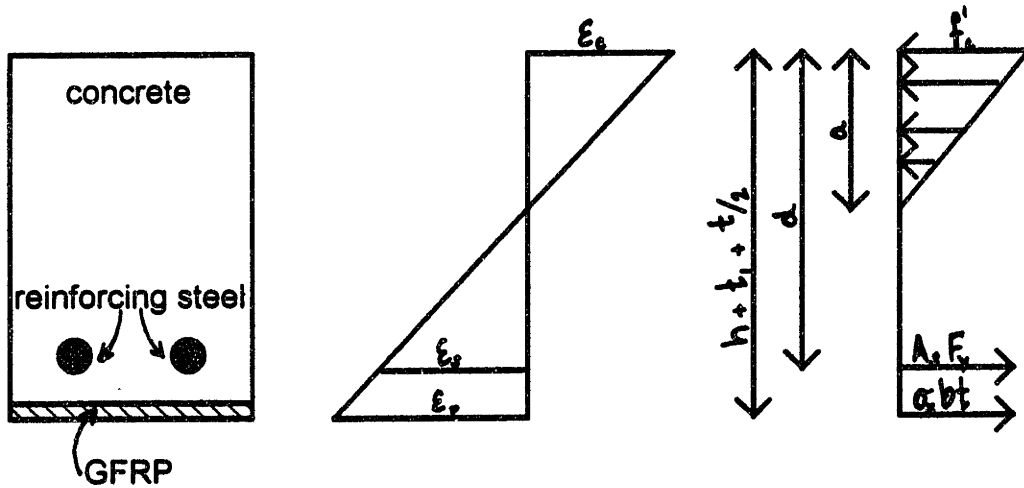| Specimen	Maximum load kN (lbs)	Strain at maximum load	Maximum stress MPa (psi)
1	1.389 (312.3)	5.216%	109.38 (15864)
2	1.364 (306.7)	5.455%	107.41 (15578)
3	1.374 (308.9)	5.605%	108.20 (15692)
4	1.379 (310.0)	5.769%	108.59 (15749)
5	1.383 (310.9)	5.638%	108.91 (15795)
Average	1.378 (309.8)	5.537%	108.50 (15736)
Standard deviation	0.00947 (2.1)	0.211%	0.75 (108)

Figure 3.1 Beam design

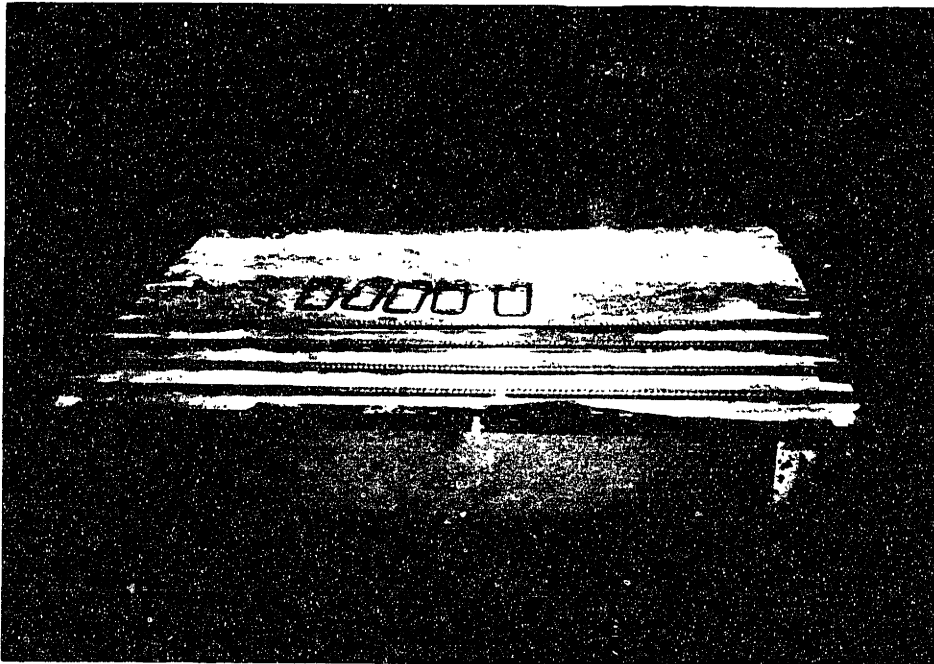Figure 3.2 Stress and strain distribution on the retrofitted cross section

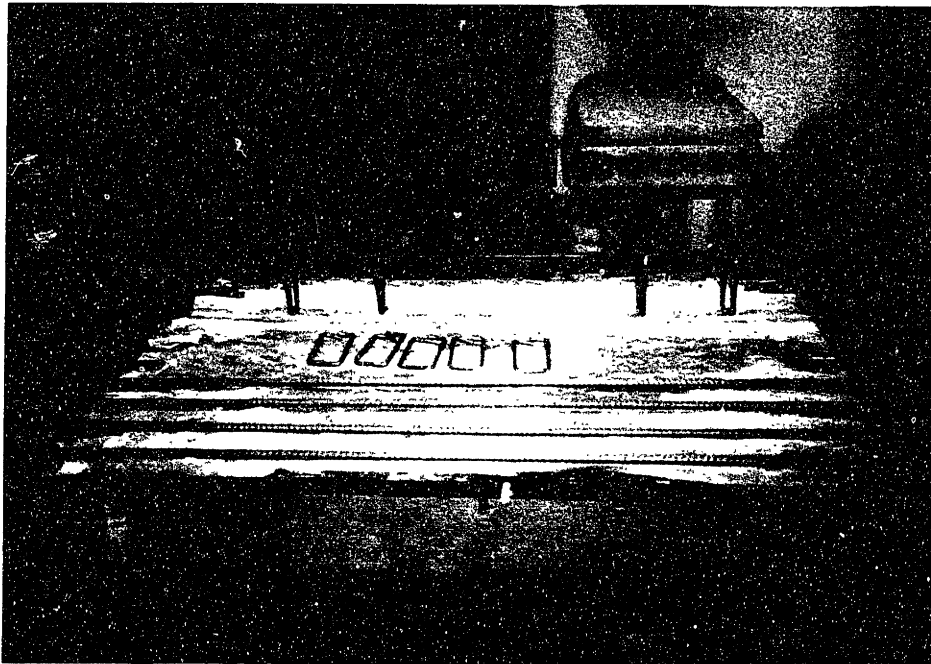Figure 3.3 Longitudinal bars and stirrups

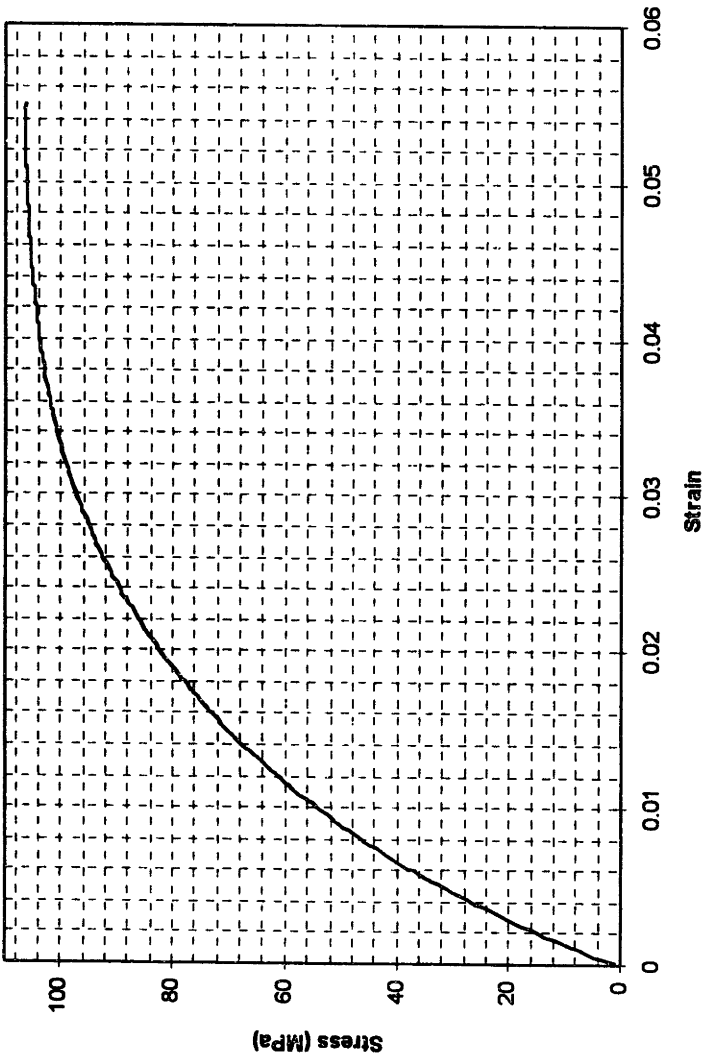Figure 3.4 Steel cage in preparation for casting.

Figure 3.5 Typical stress-strain curve of the GFRP
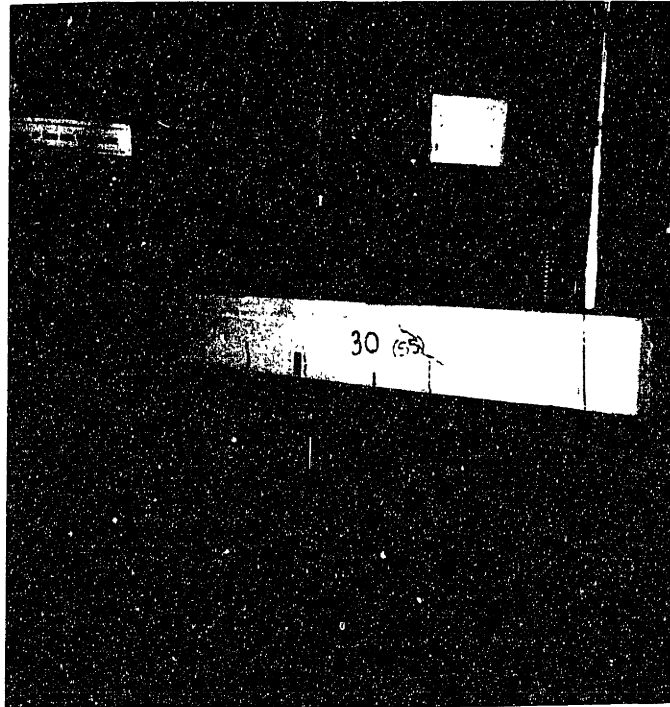
Figure 3.7 Beam in testing machine ready to be tested

Figure 3.8 Pre-cracked specimen with cracks drawn in

Chapter 4 Experimental Results and Discussion

This chapter presents and discusses the experimental results.

4.1 Raw data

This section presents the raw experimental results. Table 4.1 shows the data noted during the experiment. The beams were weighed immediately after they were removed from the curing tank and the surface wiped dry with paper towels. The beam density was consistent with the 150 pcf (2400 kg/m^3) for reinforced concrete used for calculations by the ACI Code. An explanation of the designation of each beam can be found in section 3.1.3. The pre-crack load was measured as the maximum load when the beams were pre-loaded to a midspan displacement of 0.15 inches (3.8 mm). The failure load was the maximum load achieved by the beam when tested to failure. The corresponding displacement at that maximum load was extracted from the data and included in the table. Along with each set of four beams, a set of three 3 in. x 6 in. (7.6 cm x 15 cm) cylinders were tested for compressive strength. The average strength of the three cylinders is given in the last column of the table. The cylinder strengths corresponding to each set of beams are given in Table 4.2. Overall, average concrete strength was 5084 psi. Figure 4.1 shows a typical load-displacement diagram of the beam, including the pre-load cycle. Note the gain in stiffness in the second loading cycle, indicating the presence of the GFRP plate acting as an external reinforcement. In addition, note also that delaminations of the GFRP show up on the plot as sudden drops in the load. From this point on, the pre-load cycle of the load-displacement plot will be omitted so that the graphs can be presented more clearly.

In the last three sets, the load and displacement was acquired by a plotter because the data acquisition system was not working. The plots were scanned using a Macintosh application called Ofoto. Then, the scanned plots were digitized by another Macintosh application called NIH Image, Version 1.59. The digitization of these plots allowed them to be reproduced and overlapped for comparative purposes.

4.2 Description of failure modes

The failure modes of the beams tested in the experimental program were categorized into six types of failures. Table 4.3 indicates the failure mode of each beam. This section discusses them in detail. Further analysis of the failure modes and possible correlations to the variables in the experiment is done in the following section.

Concrete crushing at midspan is one of the expected modes of failure because the addition of the GFRP creates the possibility of over-reinforcing the beam. Of the 32 beams tested, only two beams failed in this mode, Beams 18 and 25. Note that both beams failed with relatively high ductility; the displacement at failure was well over 0.4 inches (1.0 cm). Figure 4.2 shows a picture of one of beams that failed when the concrete crushed.

A drastic shear failure is the failure due to the propagation of a single, relatively straight shear crack from the tension side of the beam to the compression side of the beam. The crack often initiated very close to the support. In analyzing the failed specimen, the crack often initiated right next to the stirrup closest to the support. It then propagated diagonally up the top of the next stirrup. This failure often occurs with little ductility, showing low displacement at failure load, for example beam 34 had a displacement of only 0.262 inches (6.66 mm). This failure occurred with little or no GFRP peeling. Figure 4.3 shows a picture of the failure of a beam in this mode. The most likely cause of this failure mode is that the stirrups were spaced to far apart to be effective in arresting shear cracks.

A very common mode of failure was the failure of the layer of concrete between the GFRP and the steel reinforcing bar. This mode of failure occurred in 10 out of the 24 retrofitted beams. Figure 4.4 shows a picture of this particular type of failure. The area that was initially designed as concrete cover for the steel has become a vital part of the mechanism for the success of this retrofit method. Without the effectiveness of this layer of the concrete, the GFRP becomes ineffective. Note how the crack propagated along the length of the steel flexural reinforcement. This mode of failure occurs because of the high stress concentration at the ends of the GFRP. Other researchers have also reported this problem in almost all of the articles published on the use of GFRP's (Saadatmanesh and Ehsani 1990, Ritchie et al 1991, Saadatmanesh and Ehsani 1991, Arduini et al 1994, Sharif et al 1994). Note that this mode of failure often involved little or not delamination, indicating that the integrity of the interface was not damaged. Further analysis of this failure mode is discussed in Chapter 5.

Another mode of failure was the propagation of the flexural-shear crack. Figure 4.5 shows a picture of a beam that failed in this mode. The propagation of the crack towards the tension side of the beam often caused the GFRP to peel off. In addition, this crack can also propagate to the load point, undermining the strength of the concrete in that region. One outcome is that the concrete crushes at the load point also. As shown in the figure, the crack undermines the strength of the concrete at the load point, causing the concrete to crush. This type of failure allowed acceptable ductility in the failure of the beams.

Shear crushing also occurred in the failure of two beams. This type of failure is very similar to the behavior of a deep beam in which the locations of high shear acts in compression and crushes the concrete. Figure 4.6 shows a picture of that failure. Note the series of short shear cracks in the shear span on the far side of the beam indicating crushing in the high shear area. The small differential movement caused by the large shear crack also caused some delamination of the GFRP from the concrete.

The final type of failure mode is a shear failure with crushing at the load point. This mode of failure is very similar to the propagation of the flexural-shear crack that caused crushing at load points. The difference is that these cracks were shear cracks. Unlike drastic shear failure, these cracks were influenced by the stirrups, as indicated by the curved cracks. The stirrups were effective in arresting some shear cracks, as indicated by higher displacements attained at failure. Figure 4.7 shows a picture of this type of failure mode. Again, the propagation of the crack to the tension face of the beam may cause some delamination of the GFRP. In addition, the propagation of the crack to the compressive zone, particularly to the area of loading, undermines the strength of the concrete, causing crushing of the concrete.

4.3 Load vs. displacement at midspan plots

As mentioned in section 4.2, Figure 4.1 shows a typical load vs. displacement plot that shows both the pre-crack and failure load-displacement paths. For clearer presentation of the plots, the load vs. displacement plots used for the rest of this chapter will not show the pre-load cycle. Since the plots can be difficult to read when all 32 beams are overlapped, they will be presented grouped by the length of the GFRP so groups of 12 beams will be presented in each plot. However, to compare the different trends due to the differences in the length of the GFRP, the load vs. displacement plot of a representative beam from each designation will be

selected. In this plot, only eight beams will be presented. Further analysis of the beam behavior continues with a quantitative and qualitative analysis of the failure load, displacement at failure load, and the failure mode of the beams in the following section.

4.4 Trends in beam strengths and failure mode

In this section, the beams are grouped, and expected and unexpected trends are discussed. In addition to presenting the data points, the averages, and the standard deviation, the statistical confidence interval will also be used to show the significance or the lack of significance of the differences. To be able to do these statistical calculations, the data is assumed to be normally distributed and the sample standard deviation is assumed to be the population standard deviation (Devore 1991). Differences are considered significant at the 95% confidence level, unless noted otherwise. Reference to the failure modes can be made to Table 4.3 and Figures 4.3 to 4.7.

4.4.1 Stirrup spacing

Recall that in the initial design of the experiment, the two different stirrup spacings were designed as a variable to control crack size and shear strength of the beam. In separating the 40 beams into two categories, 5-inch (13-cm) and 7-inch (18-cm) spacings, the averages and standard deviations of the failure load and displacement at failure load were calculated and are presented in Table 4.4. The numbers showed no significant differences in any of the measured quantities. The beams with the 5-inch (13-cm) spacing were not stronger, in terms of their failure load, 7747 lbs (34.5 MN), than those with the 7-inch (18-cm) spacing, 7787 lbs (34.6 MN). They also did not show significantly greater ductility, in terms of displacement at failure load. Figure 4.8 shows the load vs. displacement for the unretrofitted beams. The solid lines represent the beams with the 5-inch (13-cm) stirrup spacing and the dashed lines represent those with 7-inch (18-cm) spacing. Similarly, Figure 4.9 and 4.10 show the load vs. displacement plot for the beams retrofitted with 36-inch (91-cm) and 28-inch (71-cm) long GFRP, respectively. These plots showed no significant trends either. Finally, Figure 4.11 shows the displacement at maximum load vs. maximum load plot of all the beams. Note that the circles represent the 5-inch (13-cm) spacing and the triangles represent the 7-inch (18-cm)

spacing. Again, no significant trends can be drawn from this plot, thus, exhausting the quantitative analysis.

Another form of comparison is the comparison of the failure modes of the beams. Although most failure modes seemed to have a mixture of both 5-inch (13-cm) and 7-inch (18-cm) spacings as indicated by the designation of each beam, two, in particular, did not. The failure due to concrete crushing occurred only in the beams designated as S5-36-RO. Both of these beams exhibited adequate shear strength and interfacial bond strength to allow this type of failure and ductility. In contrast, drastic shear failure occurred only in the beams with 7-inch (18-cm) stirrup spacing. This indicated that these stirrups were spaced too far apart to be effective on arresting the propagation of the shear cracks.

Although the different stirrup spacings showed no quantitative differences, in terms of the strength or ductility of the beams, some failure modes were indicative of one or the other spacing. The difference between 5-inch (13-cm) and 7-inch (18-cm) may not have been significant enough to show differences in strength or behavior of the beams. Because a spacing of 7 inches (18 cm) already showed drastic shear failure, that should indicate an upper limit. However, closer spacings, for example 3 inches (7.6 cm), should be explored for future experiments using beams with similar sizes to this experiment. Since stirrup spacing had no apparent affect on the strength and ductility of the beams, further analysis will discount the effect of stirrup spacing.

4.4.2 Surface texture of the GFRP

As mentioned in section 3.4, the surface of the GFRP was roughened to provide better bond with the epoxy and the concrete for some beams. Although not done for this project, the bond should be tested by simple NDT techniques, such as the impact-echo or impact resonance, to ensure that no delaminations exist prior to loading. The effectiveness of the surface texture can be discussed quantitatively and qualitatively, similar to the analysis done for the stirrup spacing.

Since stirrup spacing was discounted as an ineffective variable, the beams were divided into two groups for this analysis, those with roughened GFRP sheet and those with the smooth GFRP. Calculated averages and standard deviations are shown in Table 4.5. The beams without GFRP were excluded from the calculations, leaving 24 beams in the average and standard deviation calculations. Comparing the averages, there were no significant

differences between the roughened and smooth GFRP surface, 8125 lbs (36.1 MN) for the beams with rough GFRP as compared to 8050 lbs (35.8 MN) for beams with smooth GFRP. However, the smaller standard deviation for the smooth GFRP meant that there was more consistency, which was contrary to initial expectations. The failure load standard deviation for the smooth GFRP was half of that of the roughened GFRP. This maybe due undetected damage inflicted on the GFRP sheet from roughening up the surface or because the GFRP was not roughened evenly since that was manually done. Again, a similar graphical analysis can be done. Figure 4.12 and 4.13 show the load vs. displacement plots, similar to Figure 4.9 and 4.10, for the 36-inch (91-cm) and 28-inch (71-cm) long GFRP, respectively. This time, the beams are distinguished by the surface texture of the GFRP. In looking at the trends, the twelve plots showed no distinguishable trends. Figure 4.14 shows the displacement at maximum load vs. maximum load plot, similar to Figure 4.11, but this time, the plot distinguishes the beams by the surface texture of the GFRP. Again, this plot showed no significant trends with respect to the variable in question. The quantitative analysis shows no significant differences in strengths and ductility so further quantitative analysis will discount any differences in the surface texture of the GFRP.

Comparisons of the failure mode may give some better indications. First, note that both of the beams that failed with the concrete crushing were S5-36-RO. This may indicate that the rougher surface allowed for better bond. Of the seven beams that had significant delamination, five were retrofitted using the smooth GFRP. Again, this may have indicated better bond when the roughened GFRP was used. Even with the stronger bond, there was no increase in the beam strength or ductility. It seemed that the stronger bond only caused a change in the failure mode. With the rough GFRP, more consistency was shown in the failure mode, which may prove to be beneficial in modeling and predicting the strength of the beam. However, the trends shown here are not statistically significant enough so other aspects of the experimental variables need to be considered. It maybe concluded that the effects of the surface treatment of the GFRP is not as significant as other factors, like the type of epoxy used and the surface treatment of the concrete.

4.4.3 Length of the GFRP

Initially, the different GFRP lengths were introduced into the experiment to test the development length needed to make the GFRP effective or prevent the GFRP from

delaminating from the concrete. However, delamination was not a significant problem in this experiment. The failure modes of the beams were of greater concern. In this section, the beams will be identified by the length of GFRP or no GFRP. Table 4.6 shows the averages and standard deviations of the beams with no GFRP, 28-inch (71-cm) GFRP, and the 36-inch (91-cm) GFRP. Figure 4.15 shows overlapped plots of representative beams from each designation. They are grouped by the GFRP length or no GFRP at all. One particularly striking trend is the consistency in the stiffness of the beams retrofitted with the 28-inch (71-cm) GFRP. Similar to the trend observed in the strength from Table 4.6, the stiffness of the 28-inch (71-cm) beams was consistently higher. In addition, Figure 4.16 shows a plot of the failure load with respect to the displacement at failure load. This plot shows two trends in particular. First, note that beams with the 28-inch (71-cm) GFRP, shown by the open triangles, diamonds, squares, and circles, seemed to have attained the greatest average strength, followed by the 36-inch GFRP and the beams with no GFRP, respectively. In addition, the 28-inch (71-cm) GFRP showed much less scatter. Both of these trends were confirmed by Table 4.6. The average strength of the unretrofitted beam, at 6804 lbs (30.0 MN), was significantly lower than the retrofitted beams up to the 99% confidence level. The average failure load of the 28-inch (71-cm), 8301 lbs (36.9 MN), was higher than that of the 36-inch (91-cm), 7874 lbs (35.0 MN), at the 90% confidence level. Also, note the differences in the standard deviations. The standard deviation for both of the failure load and the displacement at failure load for the 28-inch (71-cm) GFRP were smaller than the other two groups. Part of the explanation for the higher consistency, as shown by the lower standard deviation, may be shown by an analysis of the failure mode.

Of the six observed types of failure, the beams retrofitted with the 28-inch (71-cm) long GFRP showed five. They included five failures of concrete layer between the internal and external reinforcements, three drastic shear failure, two flexural-shear crack failure, one shear crushing, and one shear failure with crushing at load point. The most dominant mode of failure was the failure of the concrete layer between the GFRP and the steel reinforcing bar. This type of failure occurs when significant stress concentrations build up at the ends of the GFRP sheets. Further analysis of this stress concentration is shown in the next chapter. In all cases, large cracks were initiated in the concrete at or near the end of the GFRP. The cracks continued to propagate to the level of the steel. Then, they either propagated along the length of the steel or met another crack causing failure of the concrete on the tension side of the beam, as shown in Figure 4.4. The area of the high stress concentration became the seed for

cracks to form and quickly propagate because concrete is weak in tension. Because the 36-inch (91-cm) GFRP extends all the way to the supports, the curvature of the beam at the end of the beam is not as significant so the interaction between the stresses is not significant. This may have alleviated this problem because it is much more pronounced with the 28-inch (71-cm) GFRP. This failure mode implicitly relies on the tensile strength of the concrete. Further discussion of this mode of failure and an analytical model is developed in Chapter 5.

4.5 Summary of the experimental program

The following is an itemized summary and concluding remarks for the experimental program.

Pre-cracking

- The beams were pre-loaded before the application of the GFRP to study the development of pre-existing cracks and their interaction with the interface between the GFRP and the reinforced concrete beam, possibly causing the delamination of the GFRP.
- The effect of pre-cracking is difficult to assess because not all cracks propagate to the surface or are large enough to be observed by the naked eye. From the observations, there were no apparent effects from the initial cracks. The delaminations that were observed were those that occurred from the propagation of large cracks developed during the final loading. The pattern of the cracks changed when the retrofitted beams were loaded. Instead of a few large cracks, smaller cracks formed more frequently along the span of the beam.
- In future experiments, nondestructive methods of detecting presence of cracks, especially those inside the beam or too small to be visible should be used. One simple test maybe to observe the changes in the wave speed of the concrete using methods such as impact-resonance or impact-echo. Because the stiffness of the concrete decreases significantly with the presence of cracks, large or small, the wave speed should echo that decrease.
- The experimental results showed that the GFRP redistributed the stress along the beam. Because the addition of the GFRP increased the stiffness of the beam, the curvature was more controlled. In addition, the GFRP took on load, relieving the stress in the steel, again controlling the strain along the soffit of the beam. Finally, the GFRP, as an external reinforcement redistributed the load such that more frequent and smaller cracks formed.

Application of the GFRP

- It has been well documented, as shown in the Literature Survey chapter, that the application of external reinforcements causes changes in the development of cracks, increase in strength and stiffness of the composite beam, and changes in the behavior of the beams at failure.

- The experimental program confirmed a number of the trends that were expected:

  ⇒ As mentioned above, the application of the GFRP onto the reinforced concrete beam caused a change in the crack pattern. In particular, instead of further development of a few large cracks incurred during the preload, numerous smaller cracks developed along the span of the beam where the GFRP was applied.

  ⇒ The retrofitted beams achieved higher strength than the unretrofitted beams. The eight unretrofitted beams had an average failure load of 6804 lbs (30.2 kN) and a standard deviation of 985 lbs (4.38kN). The 24 retrofitted beams had an average failure load of 8041 lbs (35.8 kN) and a standard deviation of 604 lbs (2.69 kN). Note that the difference between the two averages exceeded the standard deviations.

  ⇒ The increase in the stiffness of the retrofitted beams can be seen in the load vs. displacement plot. The sample plot in Figure 4.1 showed the gain in stiffness during the second loading of the beam.

  ⇒ The failure behavior of the beams changed significantly. Instead of failing in flexure, by the yielding of the steel, the retrofitted beams often failed in shear. Because of the gain in flexural strength from the addition of the GFRP, the strength of the beam was greatly influenced by the shear strength of the beam. Therefore, the failure mode of most of the retrofitted beams was dominated by the shear failure. In addition to the shear forces caused by external loads, the shear forces caused by the transfer of forces from the reinforced concrete beam to the GFRP also dominated in the failure of the beams. The stress concentration where the GFRP ended often acted as a seed for cracks to form.

- The application of the GFRP as an external reinforcement causes a number of positive gains: the gain in strength of the composite beam, the gain in stiffness of the composite beam, and the more frequent smaller cracks. However, the retrofitted beams also showed a variety of different failure modes from those observed in traditionally reinforced concrete beams. Because the different failure modes are still not well understood, predicting them

and controlling them is questionable. More importantly, the strength of the retrofitted beams cannot be predicted without a good understanding and the ability to predict the failure. The parameters possibly affecting the failure modes are discussed below and further discussed in the next chapter.

Stirrup spacing

- Two different stirrup spacings were chosen for the experimental program, namely 5-inch (13-cm) and 7-inch (18-cm). The variation in the stirrup spacings was done to study the effects of different shear strength of the beams. In addition, it was also done to provide two different levels of crack control.

- From the experimental results, there were no significant differences in terms of strength or ductility of the beams. However, some differences showed in the failure mode of the beams. Two beams with the 7-inch (18-cm) stirrup spacing failed in drastic shear because the stirrups were too far apart to arrest shear cracks. Two beams with the 5-inch (13-cm) stirrup spacing failed by crushing of the concrete. These beams showed that the 5-inch stirrup spacing was close enough to control significant shear crack propagation such that the flexural mode can dominate. However, note that this does not mean that flexural failure will always occur, as shown by the other modes of failure.

- Because the difference between the 5-inch (13-cm) and 7-inch (18-cm) spacings were not significantly different enough, there was no obvious difference in the average strengths of the beams. This parameter has the potential to rise as a significant parameter in future research. More variations of the stirrup spacings should be tested, especially those that can mimic the size ratios in real structure.

Surface texture of the GFRP

- Half of the beams were retrofitted with GFRP sheets that had been roughened with sand paper. This was done with the expectation that the rougher surface of the GFRP would allow for better bond between the reinforced concrete beam and the GFRP. The other half of the beams was retrofitted with the smooth GFRP.

- The experimental results showed no significant difference both in the strength of the beams retrofitted with the roughened or smooth GFRP. The same was found with the ductility of the beams, as shown by the average midspan displacement of at failure. However, one failure mode was apparent for the beams retrofitted with the roughened

GFRP: the failure due to the crushing of the concrete. This failure indicated good shear strength and good interfacial bond strength between the reinforced concrete beam and the GFRP because the beam was able to achieve a relatively high strength and ductility. However, note that only two of the 24 retrofitted beams failed in this manner.

- The surface texture of the GFRP may not have played a significant role in the strength or the ductility of the beams. One likely explanation is that other experimental parameters dominated in determining the strength of the bond between the reinforced concrete beam and the GFRP. Other parameters may include the surface treatment of the concrete, the shear stiffness of the epoxy, and the thickness of the epoxy. The quantitative parameters, those involving the epoxy, will be discussed in the next chapter.

Length of the GFRP

- In many practical situations, the size of the FRP sheets applied to the structure is often limited to keep the cost low. In this experiment, the length of the GFRP was varied between 28-inch (71-cm) and 36-inch (91-cm) to study any significant effects on the variation in the length. One of the problems observed by a number of other research groups is the failure of the concrete layer between the internal and external reinforcements (Ritchie 1991, Saadatmanesh and Ehsani 1990, Saadatmanesh 1991, Sharif 1994). This failure greatly undermines the strength and ductility of the beams. It has been hypothesized that the stress concentration at the end of the GFRP is the likely cause of this failure mode and maybe solved by extending the GFRP further towards the support.

- The experimental results showed distinct differences among the beams retrofitted with the 36-inch (91-cm) GFRP, 28-inch (71-cm) GFRP, and no GFRP. In particular, the beams retrofitted with the 28-inch (71-cm) GFRP showed the highest and most consistent average strength, followed by those with the 36-inch (91-cm) GFRP, and then the unretrofitted beams. However, there were no significant differences in the displacement at failure load between the beams retrofitted with the 28-inch (71-cm) and 36-inch (91-cm) GFRP. The failure modes of the beams retrofitted with the 28-inch (71-cm) GFRP echoed the results of other studies with the failure of the concrete layer between the internal and external reinforcements dominating.

- A number of conclusions and remarks can be drawn from this set of data:
  - ⇒ The beams with the 36-inch (91-cm) GFRP did not achieve the highest average load. However, the failure of the concrete layer between the internal and external

reinforcements was largely avoided. The cost for this avoidance was the scatter in the strength and the modes of failure of these beams. The experiment seems to show that by avoiding one mode of failure, i.e. the failure of the concrete layer between the external and internal reinforcements, a larger set of possible failure modes surfaced.

⇒ The beams with the 28-inch (71-cm) GFRP showed both the highest average strength and the greatest consistency in its distribution of failure loads. This is primarily from more consistency in the failure modes of the beams. However, note that the marked increase in strength was not accompanied by an increase in displacement at failure mode.

⇒ Because the beams with the 28-inch (71-cm) GFRP showed much higher consistency, the shorter GFRP length seems to show two significant advantages, based on this experiment: lower cost and higher and more consistent strength. However, the failure mode in question is not well understood and cannot be predicted. One solution is to better understand the failure mode in question by performing a parametric analysis. The stress concentration at the end of the GFRP will be further studied in the next chapter.

Table 4.1 Experimental results of beam loading

No.	Weight lbs. kg	Length inches m	Density pcf kg/m³	Designation	Pre-crack load lbs MN	Failure load lbs. MN	Displacement at failure load inches mm	Average cylinder psi MPa
1	58.75 26.6	45.25 1.14	149.57 2395	S7	3990 17.7	7230 32.2	0.4358 11.07	5159 35.6
2	60.00 27.2	45.50 1.15	151.91 2433	S7	4400 19.6	6780 30.2	0.3637 9.24	5159 35.6
3	61.19 27.7	44.75 1.13	157.52 2523	S5	4460 19.8	6480 28.8	0.3379 8.58	5159 35.6
4	57.44 26.0	43.75 1.11	151.24 2422	S5	5670 25.2	7780 34.6	0.3154 8.01	5159 35.6
5	55.50 25.1	42.00 1.07	152.23 2438	S7	5880 26.2	8400 37.4	0.3354 8.52	4631 31.9
6	56.50 25.6	42.00 1.07	154.97 2482	S7	4440 19.7	6580 29.3	0.3809 9.67	4631 31.9
7	56.50 25.6	42.00 1.07	154.97 2482	S5	3820 17.0	5500 24.5	0.3019 7.67	4631 31.9
8	56.50 25.6	42.00 1.07	154.97 2482	S5	4880 21.7	5685 25.3	0.2299 5.84	4631 31.9
17	54.50 24.7	42.00 1.07	149.49 2394	S5-36-SM	5300 23.6	7560 33.6	0.3737 9.49	5637 38.9
18	57.00 25.8	42.00 1.07	156.34 2504	S5-36-RO	5300 23.6	9300 41.4	0.4793 12.17	5637 38.9
19	54.00 24.4	42.00 1.07	148.11 2372	S7-36-RO	4780 21.3	7240 32.2	0.3544 9.00	5637 38.9
20	54.70 24.8	42.00 1.07	150.03 2403	S7-36-SM	5090 22.6	8240 36.7	0.4217 10.71	5637 38.9
21	57.00 25.8	42.00 1.07	156.34 2504	S7-36-SM	5650 25.1	8150 36.3	0.3489 8.86	4613 31.8
22	56.00 25.402	42.00 1.07	153.60 2460	S5-36-SM	5260 23.4	7920 35.2	0.3529 8.96	4613 31.8
23	56.00 25.402	42.00 1.07	153.60 2460	S5-36-RO	5520 24.6	8040 35.8	0.2919 7.41	4613 31.8
24	55.50 25.175	42.00 1.07	152.23 2438	S7-36-RO	5160 23.0	7880 35.1	0.3337 8.48	4613 31.8
25	56.00 25.402	42.00 1.07	153.60 2460	S5-36-RO	5700 25.4	8560 38.1	0.4240 10.77	5623 38.8
26	55.50 25.175	42.00 1.07	152.23 2438	S5-36-SM	5260 23.4	8190 36.4	0.3854 9.79	5623 38.8
27	58.50 26.536	42.00 1.07	160.46 2570	S7-36-RO	4840 21.5	5440 24.2	0.2157 5.48	5623 38.8
28	57.00 25.855	42.00 1.07	156.34 2504	S7-36-SM	5340 23.8	7970 35.5	0.2752 6.99	5623 38.8
33	57.00 25.855	42.00 1.07	156.34 2504	S7-28-SM	5570 24.8	9260 41.2	0.4838 12.29	4913 33.9
34	59.00 26.762	42.00 1.07	161.83 2592	S7-28-RO	5770 25.7	9040 40.2	0.3231 8.21	4913 33.9
35	56.00 25.402	42.00 1.07	153.60 2460	S5-28-RO	5350 23.8	8730 38.8	0.3293 8.36	4913 33.9
36	56.00 25.402	42.00 1.07	153.60 2460	S5-28-SM	4950 22.0	8020 35.7	0.2981 7.57	4913 33.9
37	56.50 25.628	42.00 1.07	154.97 2482	S7-28-SM	5550 24.7	7480 33.3	0.2528 6.42	5043 34.8
38	59.00 26.762	42.00 1.07	161.83 2592	S7-28-RO	5850 26.0	8420 37.5	0.3574 9.08	5043 34.8
39	56.00 25.402	42.00 1.07	153.60 2460	S5-28-SM	5870 26.1	8650 38.5	0.3215 8.17	5043 34.8
40	57.00 25.855	42.00 1.07	156.34 2504	S5-28-RO	5760 25.6	8170 36.3	0.3371 8.56	5043 34.8
41	56.00 25.402	42.00 1.07	153.60 2460	S7-28-RO	5380 23.9	8920 39.7	0.3309 8.40	4869 33.6
42	59.00 26.762	42.00 1.07	161.83 2592	S7-28-SM	5140 22.9	7560 33.6	0.2622 6.66	4869 33.6
43	57.00 25.855	42.00 1.07	156.34 2504	S5-28-SM	5300 23.6	7600 33.8	0.3153 8.01	4869 33.6
44	56.00 25.402	42.00 1.07	153.60 2460	S5-28-RO	5200 23.1	7760 34.5	0.3309 8.40	4869 33.6

54

Table 4.2 Cylinder strengths

Set	Cylinder 1 psi (MPa)	Cylinder 2 psi (MPa)	Cylinder 3 psi (MPa)	Average psi (MPa)	Standard deviation psi (MPa)
1	4810 (33.2)	5411 (37.3)	5256 (37.3)	5159 (35.6)	312 (2.2)
2	4442 (30.6)	4994 (30.6)	4456 (34.4)	4630 (31.9)	315 (2.2)
3	5192 (35.8)	5715 (35.8)	6005 (39.4)	5637 (38.9)	412 (2.8)
4	4680 (32.3)	4640 (32.3)	4520 (32.0)	4613 (31.8)	83.3 (0.6)
5	5751 (39.7)	5383 (39.7)	5737 (37.1)	5624 (38.8)	209 (1.4)
6	5319 (36.7)	4463 (36.7)	4958 (30.8)	4913 (33.9)	430 (3.0)
7	4731 (32.6)	5223 (32.6)	5176 (36.0)	5043 (34.8)	272 (1.9)
8	4838 (33.4)	4771 (33.4)	4997 (32.9)	4869 (33.6)	116 (0.8)

Table 4.3 Failure modes of the beams

	Designation	Pre-crack load lbs kN	Failure load lbs kN	Displacement at failure load inch mm	Delamination?	Failure mode
25	S5-36-RO	5700 25.4	8560 38.1	0.4240 10.77	no	Concrete crushing
18	S5-36-RO	5300 23.6	9300 41.4	0.4793 12.17	no	Concrete crushing
27	S7-36-RO	4840 21.5	5440 24.2	0.2157 5.48	no	Drastic shear failure
42	S7-28-SM	5140 22.9	7560 33.6	0.2622 6.66	limited	Drastic shear failure
34	S7-28-RO	5770 25.7	9040 40.2	0.3231 8.21	no	Drastic shear failure
36	S5-28-SM	4950 22.0	8020 35.7	0.2981 7.57	no	Drastic shear failure - some shear crushing; flexural-shear crack does not propagate
19	S7-36-RO	4780 21.3	7240 32.2	0.3544 9.00	yes	Failure of concrete between plate and rebar
43	S5-28-SM	5300 23.6	7600 33.8	0.3153 8.01	no	Failure of concrete between plate and rebar
44	S5-28-RO	5200 23.1	7760 34.5	0.3309 8.40	no	Failure of concrete between plate and rebar
28	S7-36-SM	5340 23.8	7970 35.5	0.2752 6.99	no	Failure of concrete between plate and rebar
23	S5-36-RO	5520 24.6	8040 35.8	0.2919 7.41	no	Failure of concrete between plate and rebar
38	S7-28-RO	5850 26.0	8420 37.5	0.3574 9.08	no	Failure of concrete between plate and rebar
35	S5-28-RO	5350 23.8	8730 38.8	0.3293 8.36	no	Failure of concrete between plate and rebar
41	S7-28-RO	5380 23.9	8920 39.7	0.3309 8.40	no	Failure of concrete between plate and rebar
20	S7-36-SM	5090 22.6	8240 36.7	0.4217 10.71	yes	Flexural - shear crack failure
39	S5-28-SM	5870 26.1	8650 38.5	0.3215 8.17	yes	Flexural - shear crack failure
33	S7-28-SM	5570 24.8	9260 41.2	0.4838 12.29	limited	Flexural - shear crack failure
37	S7-28-SM	5550 24.7	7480 33.3	0.2528 6.42	limited	Shear crushing
17	S5-36-SM	5300 23.6	7560 33.6	0.3737 9.49	limited	Shear crushing
24	S7-36-RO	5160 23.0	7880 35.1	0.3337 8.48	yes	Shear failure; crushing at load point
22	S5-36-SM	5260 23.4	7920 35.2	0.3529 8.96	yes	Shear failure; crushing at load point
21	S7-36-SM	5650 25.1	8150 36.3	0.3489 8.86	yes	Shear failure; crushing at load point
40	S5-28-RO	5760 25.6	8170 36.3	0.3371 8.56	no	Shear failure; crushing at load point
26	S5-36-SM	5260 23.4	8190 36.4	0.3854 9.79	yes	Shear failure; crushing at load point

Table 4.4 Averages grouped by different stirrup spacings

	5-inch (13-cm) spacing		7-inch (18-cm) spacing	
	average	standard deviation	Average	standard deviation
Failure load lbs (MN)	7747 (34.5)	1045 (4.65)	7787 (34.6)	997 (4.44)
Displacement at failure load inches (mm)	0.339 (8.61)	0.057 (1.5)	0.342 (8.69)	0.069 (1.77)

Table 4.5 Averages grouped by different GFRP surface texture

	Rough GFRP		Smooth GFRP	
	average	standard deviation	average	standard deviation
Failure load lbs (MN)	8125 (36.1)	1030 (4.58)	8050 (35.8)	515 (2.29)
Displacement at failure load inches (mm)	0.342 (8.69)	0.0641 (1.62)	0.341 (8.66)	0.0683 (1.74)

Table 4.6 Averages grouped by different GFRP length

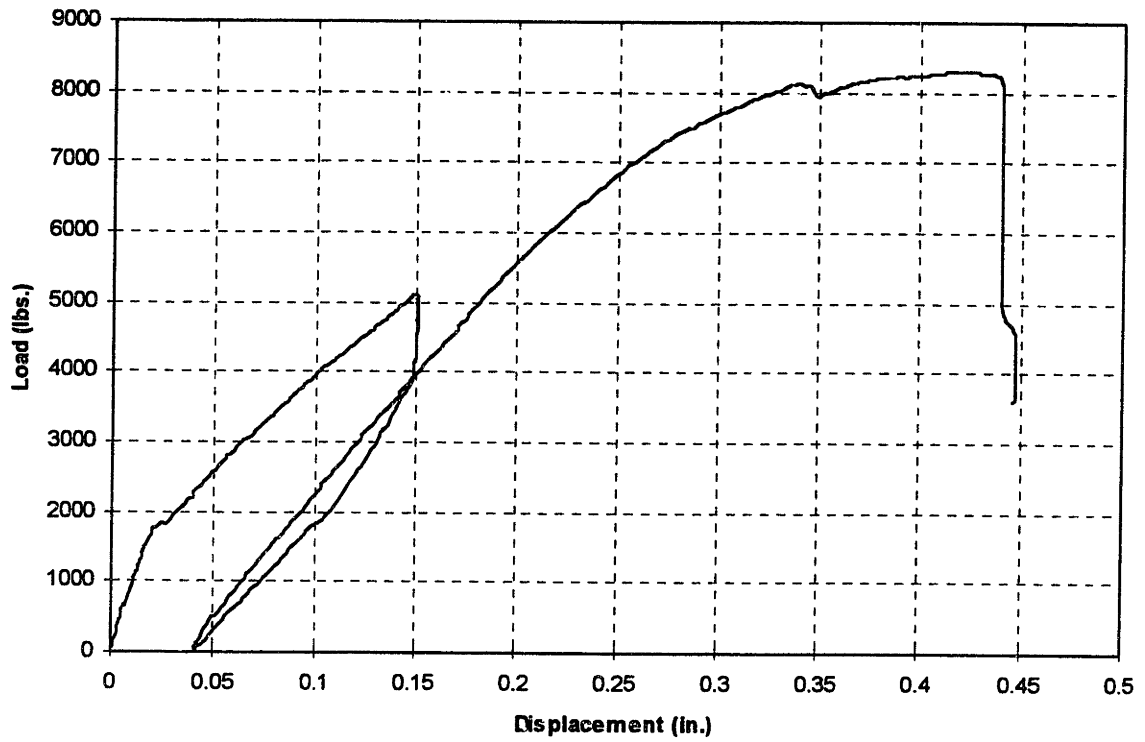|	Failure load		Displacement at failure load	
	average lbs (MN)	standard deviation lbs (MN)	average inch (mm)	standard deviation inch (mm)
No GFRP	6804 (30.3)	985 (4.38)	0.338 (8.58)	0.0604 (1.53)
28-inch (71-cm) GFRP	8301 (36.9)	623 (2.77)	0.329 (8.34)	0.0575 (1.46)
36-inch (91-cm) GFRP	7874 (35.0)	918 (4.09)	0.355 (9.01)	0.0715 (1.81)

Figure 4.1 Typical load vs. displacement diagram, including the pre-load cycle

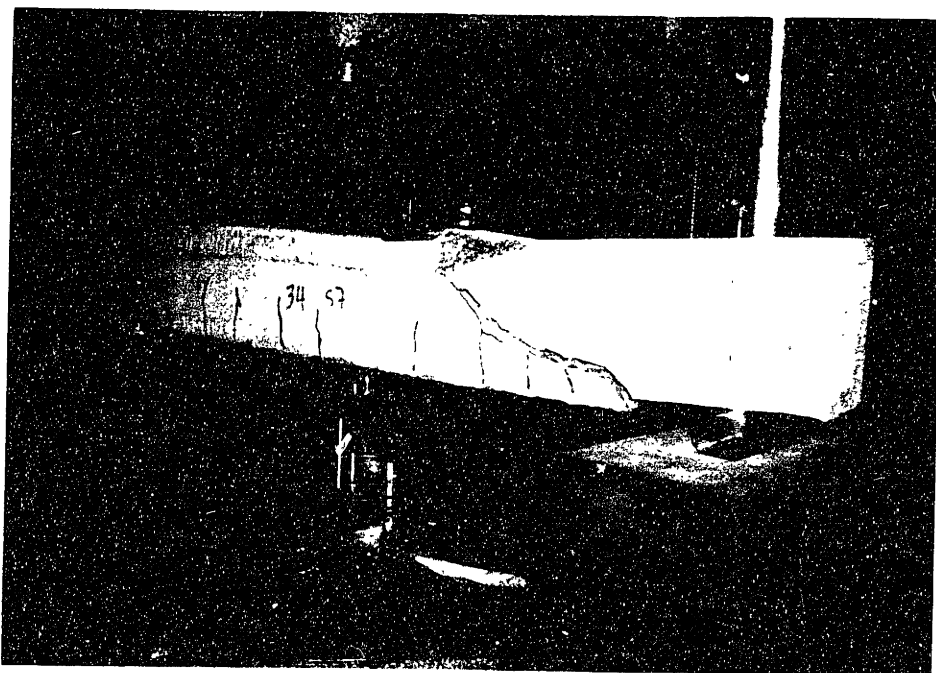Figure 4.2 Failure by concrete crushing

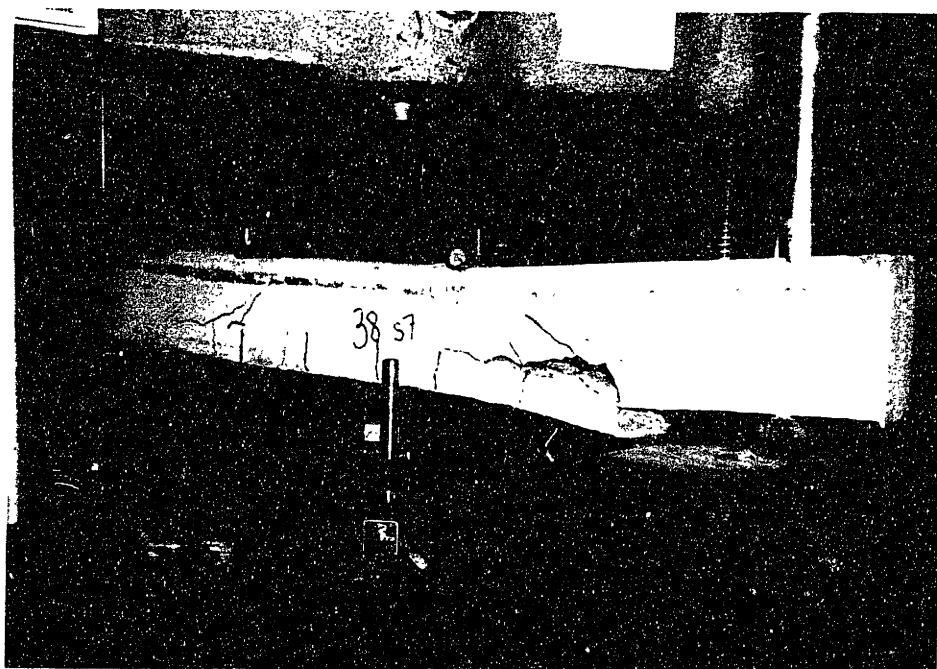Figure 4.3 Drastic shear failure

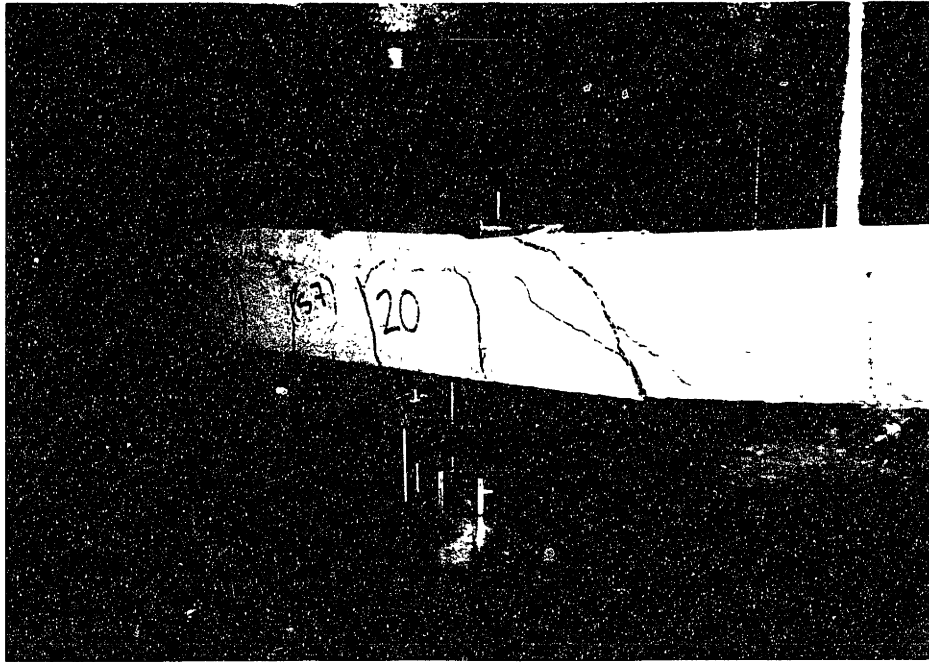Figure 4.4 Failure of the concrete layer between GFRP and steel

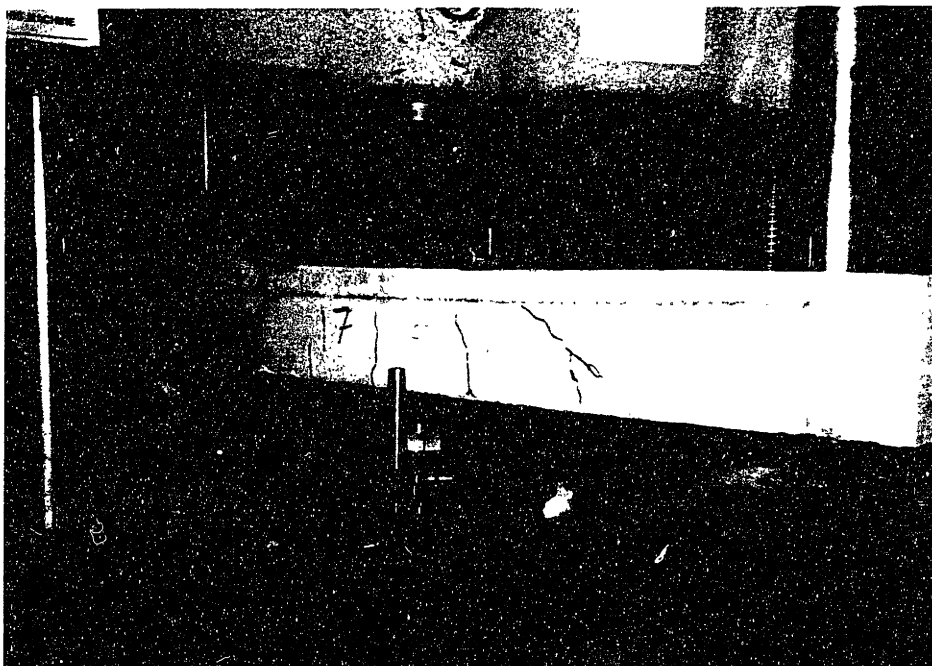Figure 4.5 Flexural due to the flexural-shear crack

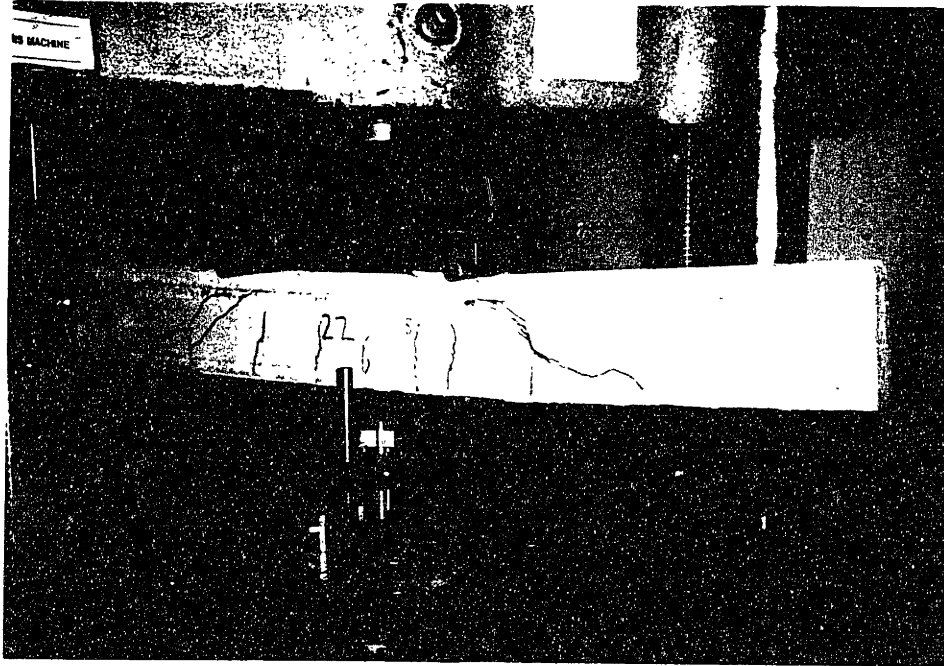Figure 4.6 Failure due to shear crushing

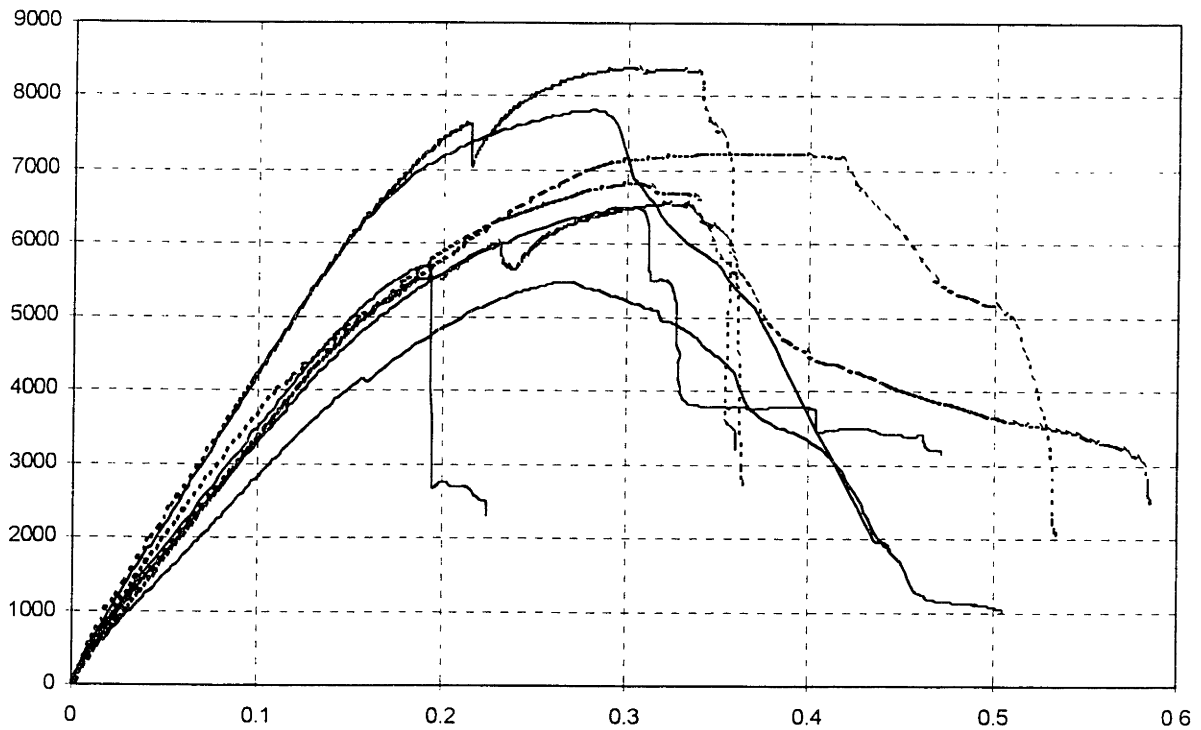Figure 4.7 Failure due to crushing at load points

Figure 4.8 Load vs. displacement plots for all unretrofitted beams
Solid lines: 5-inch (13-cm) stirrup spacing; Dashed lines: 7-inch (18-cm) stirrup spacing
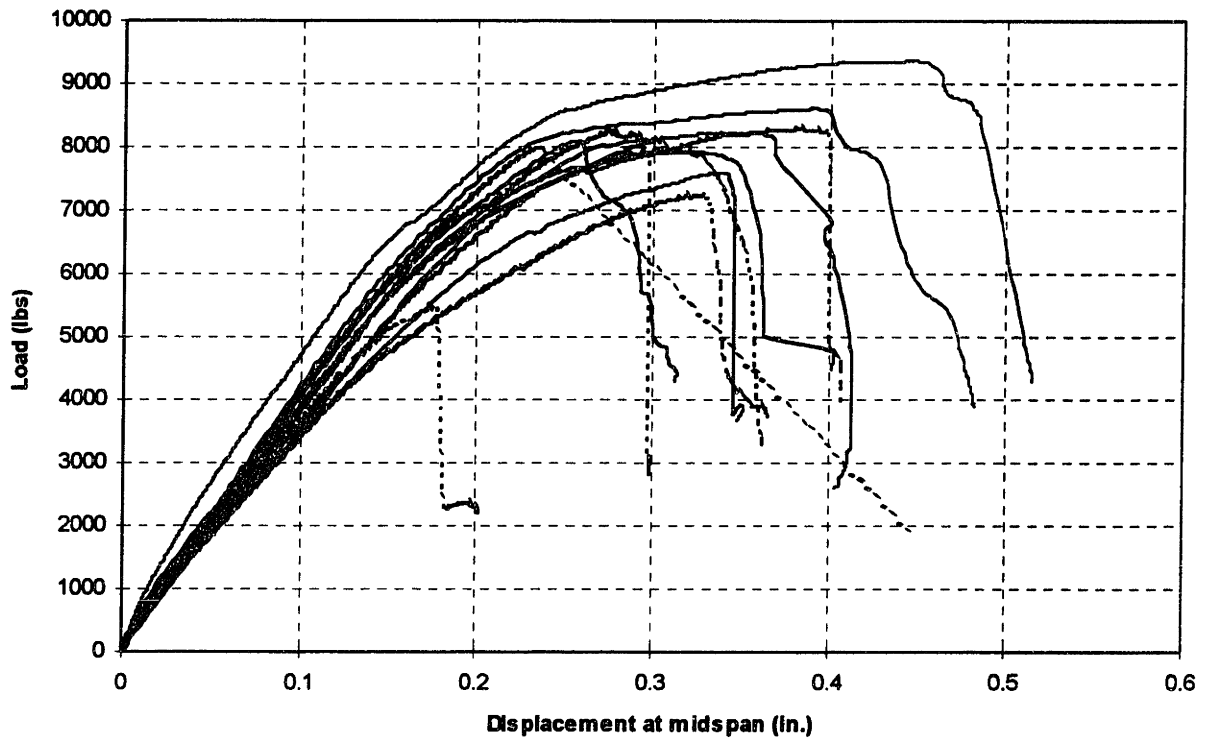
61

Figure 4.9 Load vs. displacement plots for all beams with 36-in (91-cm) GFRP
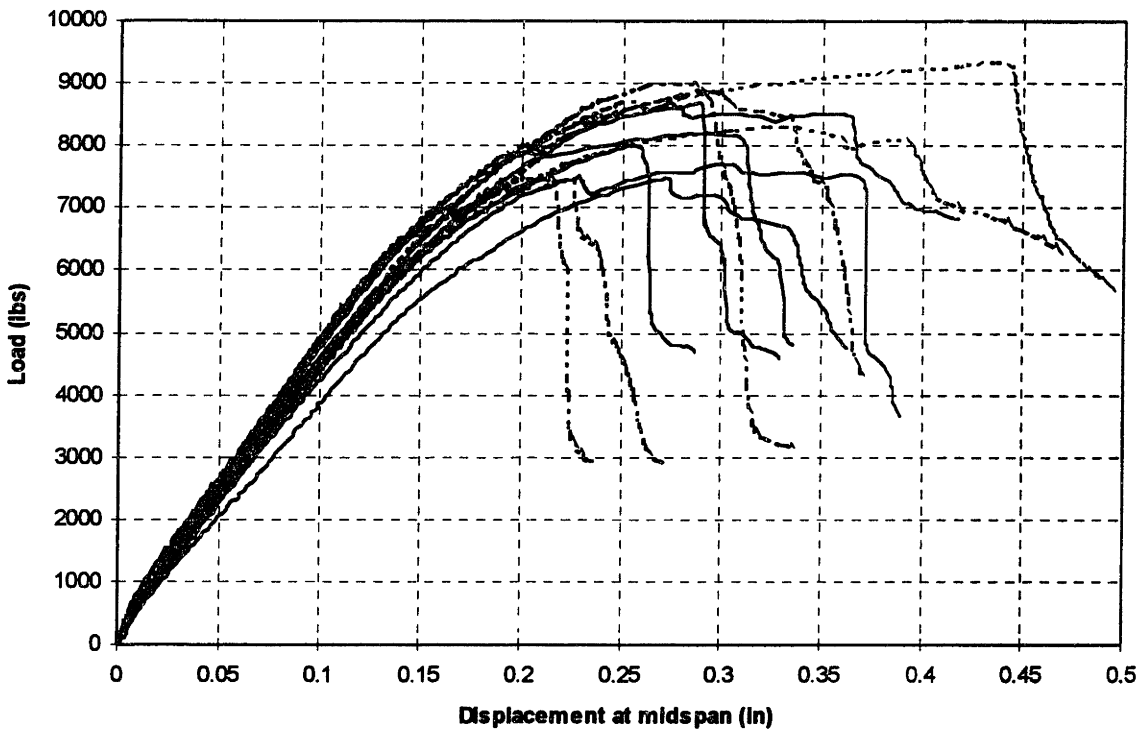Solid lines: 5-inch (13-cm) stirrup spacing; Dashed lines: 7-inch (18-cm) stirrup spacing

Figure 4.10 Load vs. displacement plots for all beams with 28-in (71-cm) GFRP
Solid lines: 5-inch (13-cm) stirrup spacing; Dashed lines: 7-inch (18-cm) stirrup spacing
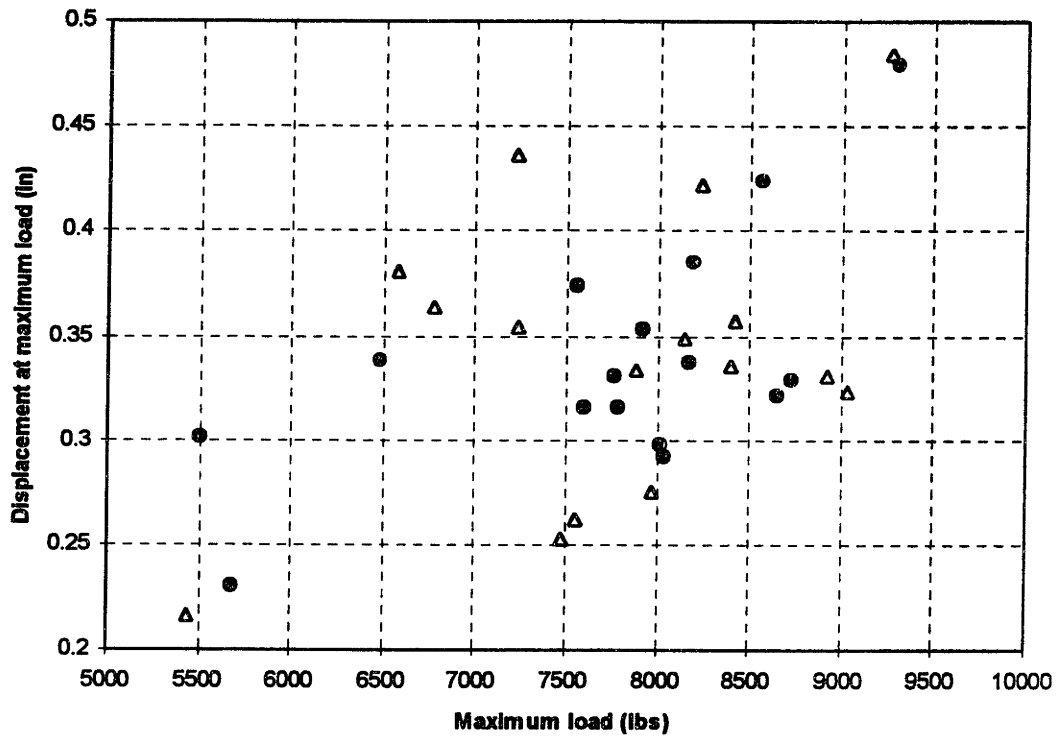
Figure 4.11 Displacement at maximum load vs. maximum load for all beams
Filled in circles: 5-inch (13-cm) stirrup spacing; Clear triangles: 7-inch (18-cm) stirrup spacing
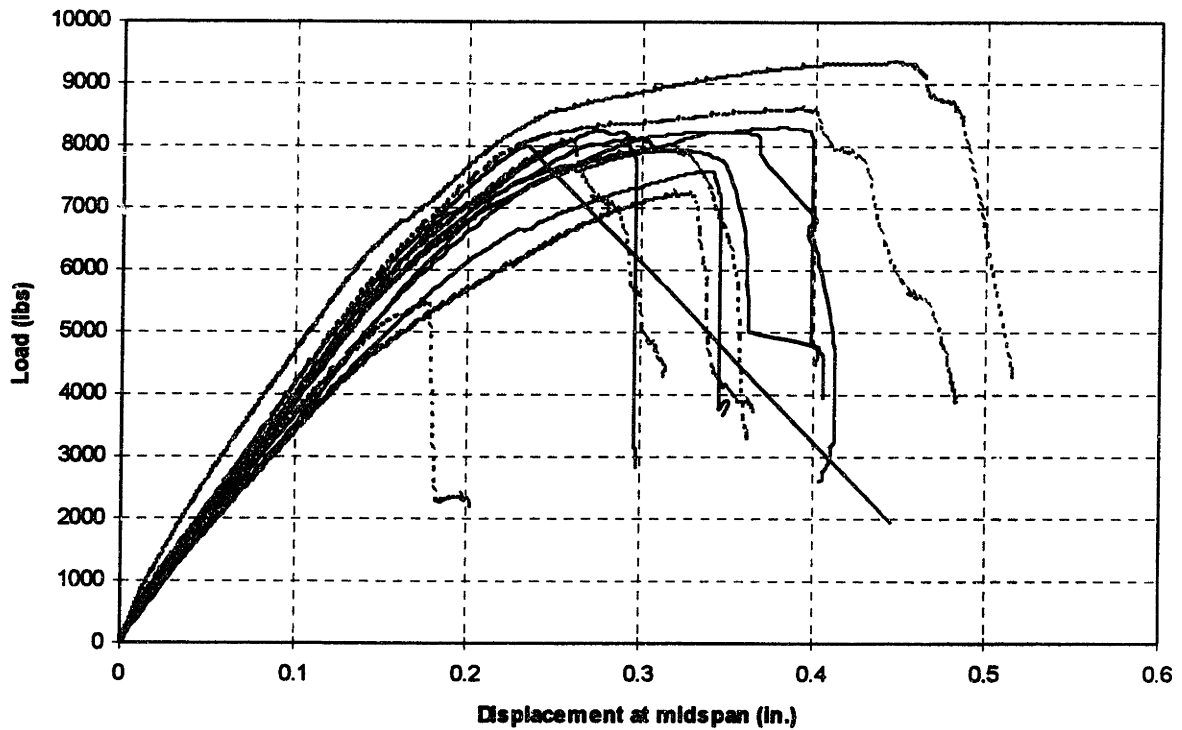

Figure 4.12 Load vs. displacement plots for all beams with 36-in (91-cm) GFRP
Solid lines: smooth GFRP; Dashed lines: rough GFRP
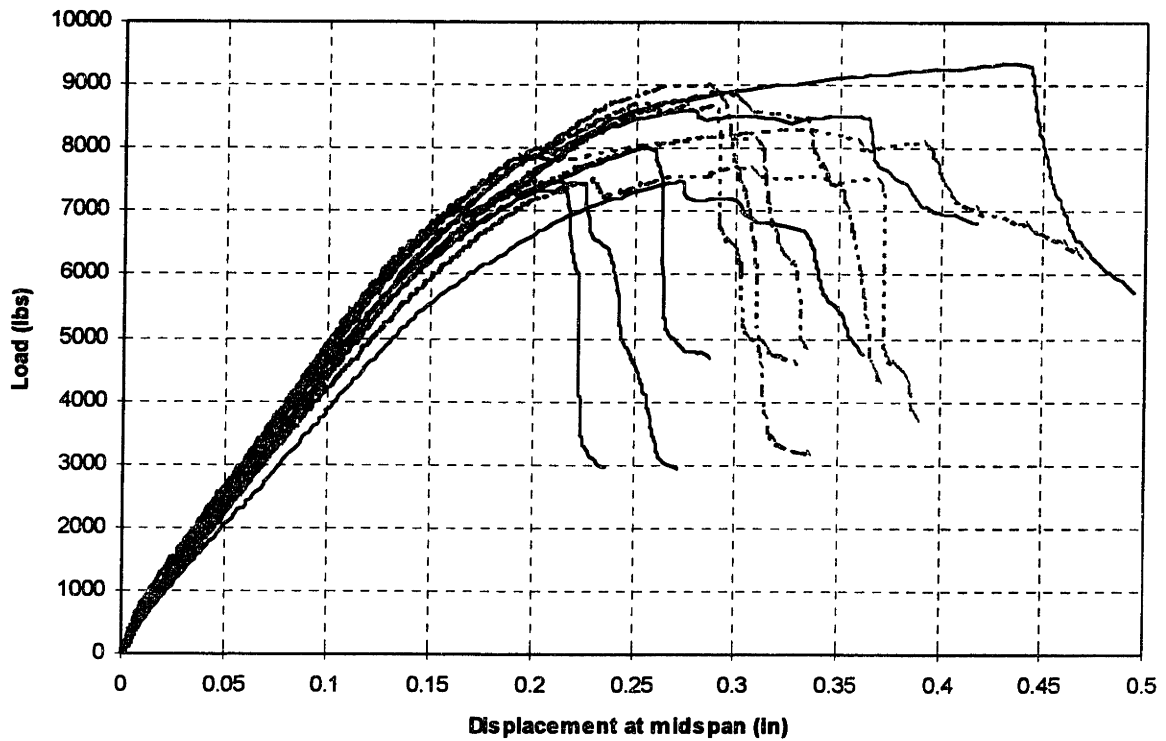
Figure 4.13 Load vs. displacement plots for all beams with 28-in (71-cm) GFRP
Solid lines: smooth GFRP; Dashed lines: rough GFRP
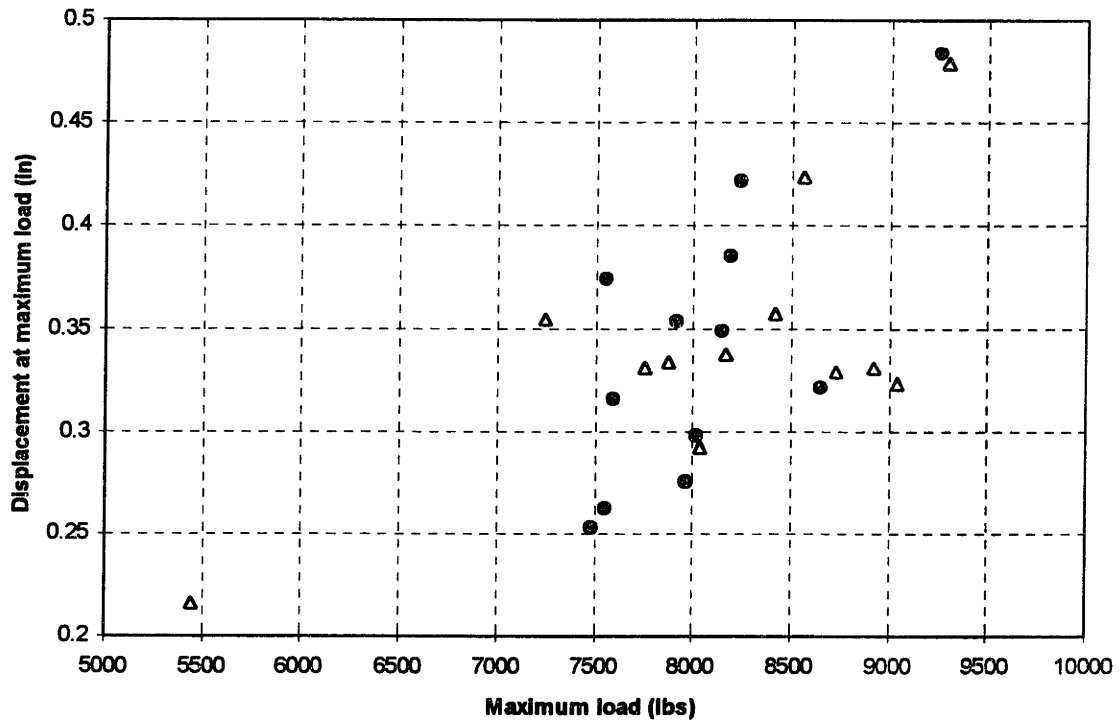
Figure 4.14 Displacement at maximum load vs. maximum load for all beams
Filled in circles: smooth GFRP; Clear triangles: rough GFRP
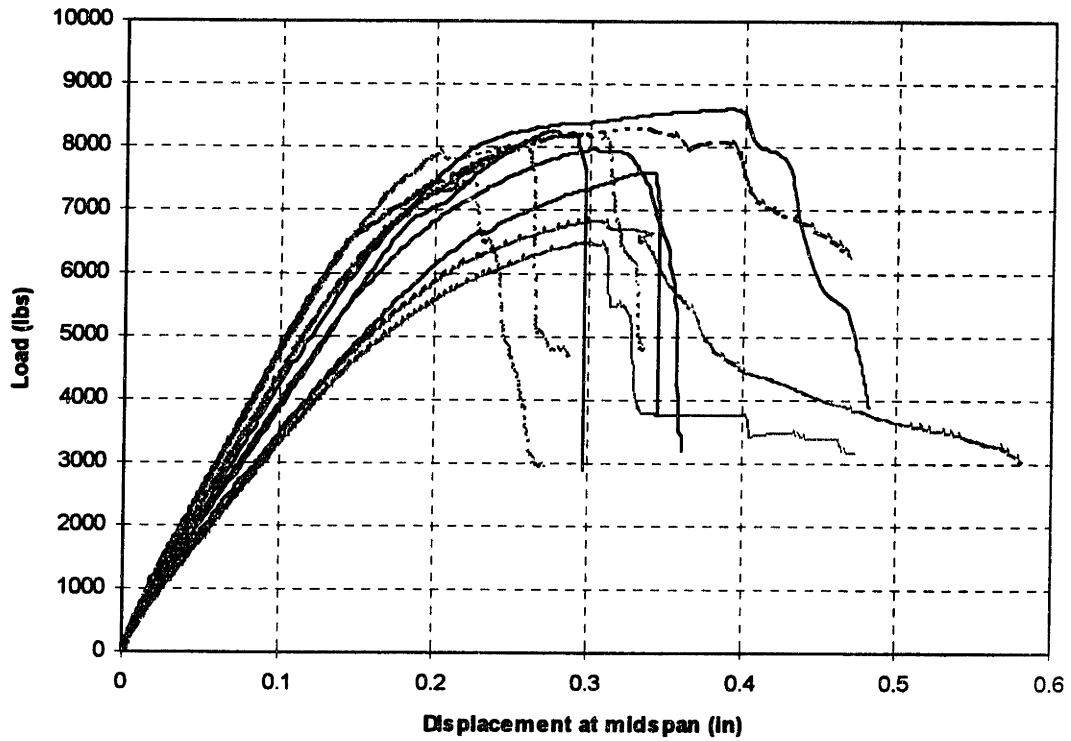
Figure 4.15 Load vs. displacement of representative beams for each beam designation
Dashed lines: 28-inch long GFRP; Solid lines: 36-inch long GFRP; Gray lines: no GFRP

X S5 X S7 ▲ S5-36-RO ◆ S5-36-SM◼ S7-36-RO ● S7-36-SM△ S5-28-RO ◇ S5-28-SM◻ S7-28-RO ○ S7-28-SM

Figure 4.16 Displacement at maximum load vs. maximum load for all beams

5 Stress distribution analysis

A stress distribution analysis of the shear stress concentration at the end of the external reinforcement will be presented in this chapter. A model will be developed to study the effects of the variation of different parameters.

5.1 Qualitative reasoning

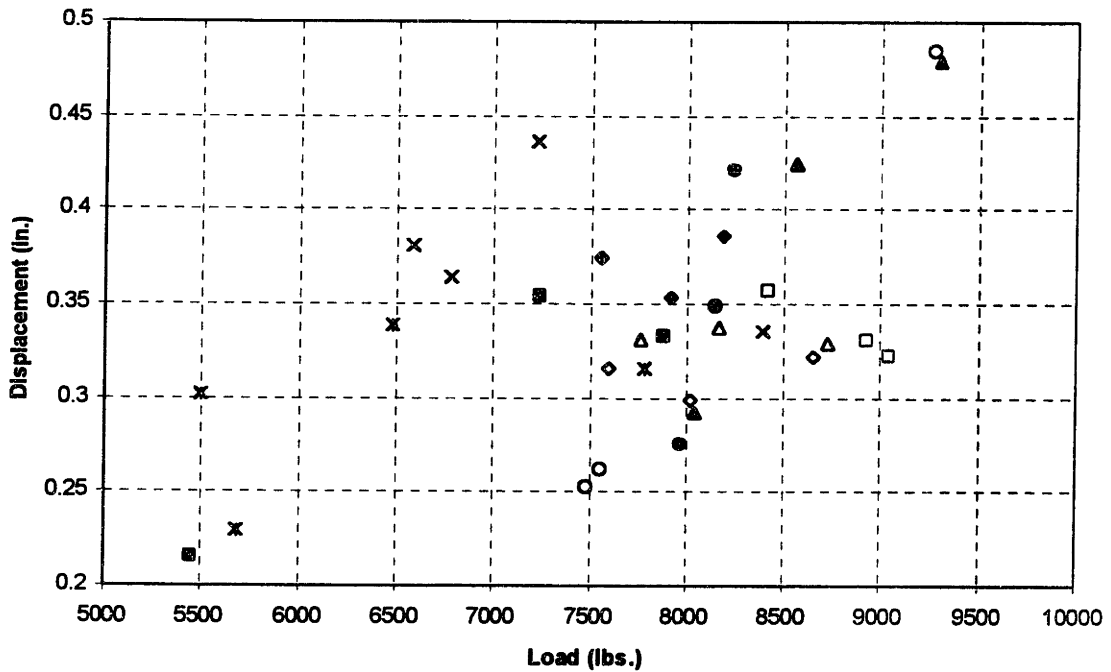The application of the GFRP on the soffit of the beam adds an extra tensile force to counteract the compressive force on the concrete. When observed more closely, the GFRP has many more effects on the reinforced concrete beam. For example, the GFRP may act to close cracks in concrete. Although cracked concrete can no longer take tensile force, the interlocking effects on the crack surface may affect the stiffness of the retrofitted beam. In addition, the elastic properties of the GFRP will also control the elastic and plastic behavior of the retrofitted concrete beam. As the beam bends, the GFRP acts in tension along the length of the beam. Like the internal steel reinforcement, the GFRP provides the tensile force to counteract the compressive force in the concrete. Although ACI code does not consider the concrete in tension to be effective, the concrete is necessary to hold the steel to the beam. When the GFRP is applied to the beam, the composite action of the whole beam will change. Properties in question are the bond of the GFRP and the mechanical properties of the GFRP. In addition, the most important question for this analysis is the stress concentration of the GFRP. Consider the following qualitative reasoning.

In mechanics, when the load is applied to the beam, the beam bends creating an internal bending moment consisting of the compressive forces from the concrete counteracted by the tensile forces from the reinforcements. If plane sections are assumed to remain plane, then the stress distribution can be calculated from the strain distribution, as shown in Figure 5.1. Assuming linear elasticity in the GFRP, the moment capacity of the section can be calculated. This assumes ideal conditions in bending, like perfect bond. Consider the stress concentration at the end of the GFRP. Within that area, the stress distribution must change

drastically. Within the area where the GFRP is still effective, the bending moment of the beam is taken on by both the composite action of the GFRP and the reinforced concrete beam. Where there is no GFRP, the moment is only resisted by the reinforced concrete beam. Although the curvature of the beam is always continuous, the change in the stiffness causes a discontinuous change in the curvature, causing a significant stress concentration at the end of the GFRP and a seed for cracks to initiate. The stress concentration within this region will be studied in the following model.

5.2 Modeling

This section will explain the model, simplifications from the actual experiment, and the parameters used. Then, the constitutive relations will be developed and the governing equations to be used in the computer program will be derived.

5.2.1 Model and parameters

The basic model is a simplified form of the beams used in the experiments. The material properties and beam dimensions are the same as those presented in Section 3.1.1. The pertinent values are as follows:

Concrete strength	$f'_c =$	5.0	ksi	34.5	GPa
Yield strength of the flexural steel	$F_y =$	50	ksi	345	GPa
Area of flexural steel	$A_s =$	0.22	in^2	1.42	cm^2
Width of beam/GFRP sheet	$b =$	3	in	7.62	cm
Distance from top of beam to flexural steel	$d =$	3.5	in	8.89	cm
Height of beam	$h =$	5	in	12.7	cm
Thickness of GFRP	$t =$	3.94 x 10^{-3}	in	1	mm
Thickness of epoxy	$t_l =$	3.94 x 10^{-4}	in	0.1	mm
Length of beam	$l_b =$	36	in	91.4	cm
Length of GFRP	$l_c =$	28	in	71.1	cm

The elastic properties are as follows:

Young's modulus of steel	$E_s =$	29,000	ksi	200	GPa
Young's modulus of concrete	$E_c =$	4,031	ksi	27.8	GPa
Young's modulus of GFRP	$E_p =$	1038	ksi	7.16	GPa
Shear modulus of the epoxy	$G =$	288	ksi	1.99	GPa

The elastic properties were either assumed or calculated. The Young's modulus of steel in this analysis is the standard value, as suggested by the ACI Code. The concrete modulus was calculated from the following equation given by the ACI Code (all values in the units of psi):

$$E_c = 57000\sqrt{f'_c}$$ (Equation 5.1)

$$E_c = 57000\sqrt{5000} = 4.031 \times 10^6 \, psi.$$

Although the GFRP had a highly non-linear stress-strain diagram, it was assumed to be linearly elastic without strain-hardening using the initial tangent modulus as the modulus of elasticity. Note that the stress in the GFRP is low enough to allow such an assumption. However, to verify the validity of this simplification, the elastic modulus of the GFRP will be varied to observe any significant changes. Linear elasticity will always be assumed. Finally, the shear modulus of the epoxy was calculated because the data was not available from the manufacturer. The published value of the Young's modulus of the epoxy was used in the calculation along with an assumed Poisson's ratio of 0.3. The following shows the calculations:

$$E_p = 7.5 \times 10^5 \, psi$$

$$v = 0.3$$

$$G = \frac{E}{2(1+v)} = \frac{7.5 \times 10^5}{2(1 + 0.3)} = 2.88 \times 10^4 \, psi.$$ (Equation 5.2)

These properties will be used with the constitutive relations to calculate the shear stress distribution along the interface between the reinforced concrete and the GFRP.

5.2.2 Constitutive relations

To calculate the shear stress distribution along the interface, constitutive relations were derived and equilibrium equations were calculated. Using the origin at the midspan of the beam, the following nomenclature will be used, as shown by Figure 5.2:

u_B = displacement of the element of the beam in contact with the epoxy;

u_c = displacement of the GFRP;

f_s = stress in the steel reinforcing bars;

τ = shear stress.;

σ_x = axial stress in the GFRP;

ε_p = axial strain in the GFRP.

The shear stress is defined as follows:

$$\tau = \frac{G(u_B - u_c)}{t_1}.$$ (Equation 5.3)

From Figure 5.3, the following stress equilibrium can be derived:

$$\frac{d\sigma_x}{dx} \times b \times t + \tau \times b \times dx = 0,$$ (Equation 5.4)

and simplified to

$$\frac{d\sigma_x}{dx} = -\frac{\tau}{t}.$$ (Equation 5.5)

Combining Equations 5.3 and 5.5, the following can be derived:

$$\frac{d\sigma_x}{dx} = -\frac{G(u_B - u_c)}{t \times t_1}.$$ (Equation 5.6)

Using the definition of strain, the following is true:

$$\sigma_x = E_p \varepsilon_p(x) = E_p \frac{du_c}{dx}.$$ (Equation 5.7)

By differentiating the stress-strain equation and assuming that the Young's modulus of the GFRP is constant throughout the length of the beam,

$$\frac{d\sigma_x}{dx} = E_p \frac{d^2 u_c}{dx^2}.$$ (Equation 5.8)

Equating Equations 5.6 and 5.8, the following governing second-order differential equation is derived:

$$E_p \frac{d^2 u_c}{dx^2} = -\frac{G(u_B - u_c)}{t \times t_1},$$ (Equation 5.9)

which simplifies into the following form of the differential equation:

$$\frac{E_p \times t \times t_1}{G} \frac{d^2 u_c}{dx^2} - u_c = -u_B.$$ (Equation 5.10)

To seed the calculations, the displacement of the beam is needed. This is calculated from the model of the beam presented in Figure 5.1. The main assumption is that plane sections remain plane. For a given load, the moment distribution can be calculated, as shown in Figure 5.4. The moment is defined at any location along the beam. In this model, a load of 5000 lbs (22 kN) will be used for all analysis. This moment is then used to calculate the u_B from the moment curvature relationship:

$$u_B = \int_0^x \frac{My}{E_c I} dx,$$ (Equation 5.11)

where:

$M =$ moment at the location x;

$y =$ distance from the neutral axis to the bottom surface of the reinforced concrete beam;

$E_c =$ the Young's modulus of the concrete;

$I =$ the section modulus of the whole composite section.

Then, Equation 5.10 is used to calculate the u_c, and Equation 5.3 is used to calculate the shear stress, given u_B and u_c. Now, u_B needs to be recalculated. Since the moment at any location along the beam is dependent only upon the external loads, the stress distribution can be recalculated using equilibrium of forces and moments. First, the stress in the GFRP must be calculated. From Equation 5.5, the following is true:

$$d\sigma_x = -\frac{\tau}{t} dx,$$

and can be rewritten as

$$\sigma_x = \int_0^x -\frac{\tau}{t} dx.$$ (Equation 5.12)

From this equation, the axial stress in the GFRP can be calculated. Using the stress distribution in Figure 5.1 and ignoring the strain distribution, the following equilibrium equations can be derived:

$$M_{ext} = \tfrac{1}{3} f'_c a^2 b + f_s A_s d + \sigma_x bt(h + t_1 + \tfrac{t}{2})$$ (Equation 5.13)

$$\tfrac{1}{2} f'_c ab = f_s A_s + \sigma_x bt$$ (Equation 5.14)

In this case, the two unknowns are f_s and a. The two equations can then be solved for a. The section modulus of the beam needs to be recalculated from the new effective concrete height, a. Then, the moment taken on by the reinforced concrete and the external reinforcement can be calculated as follows:

$$M_{\text{total}} = M_{\text{reinforced\_concrete}} + M_{\text{external\_reinforcement}} \qquad \text{(Equation 5.15)}$$

$M_{\text{external\_reinforcement}} = (\sigma_x bt) \times$ (distance from neutral axis to the middle of the external reinforcement) Since all other variables are known, the moment in the reinforced concrete section can be calculated. This can then be used to re-calculate the displacement at the bottom of the beam using Equation 5.11. With the new u_B, the calculation process begins again. This redistribution of stresses is a converging series. The Matlab script files, in the Appendix, are a numerical simulation of this model. Preliminary results had shown that after five iterations, the force in the GFRP changes by less than 1% so five iterations were used for all calculations. In addition, the stress in the steel was checked for yielding. Under an external load of 5000 lbs (22 kN), the stress in the steel was below its yield strength. Because the model was relatively simple, the stress distribution was not perfectly accurate. Figure 5.5 shows the correct form of the stress distribution, as would be calculated by more complicated models. Note that, in this diagram, the shear stress distribution is shown with the origin at the end of the external reinforcement.

5.3 Results from modeling

Modeling of the stress distribution shows that a significant stress concentration exists where the GFRP ends along the length of the beam. First, the stress distribution of the model of the experimental beam will be presented. This section will discuss the inconsistencies and problems with the simple model. The following sections show the effects of variations of a number of the experimental parameters. The experimental variables were varied one by one while all other parameters were kept at the experimental value shown above. The results from this modeling are shown. The x-axis of the graphs shows the distance from the center of the beam. Because of the high stress concentrations within a very small area, the plots often showed only a small but critical area which the change in stress concentration is significant. Note that the length of the GFRP from the middle of the beam is half the length of the whole GFRP. In most of the analysis, the GFRP ended at 0.3556 m (14 inches). The results are discussed in detail, especially in terms of possible applications in future research. The objective of this part of the project is to highlight certain properties of the experimental set-up that may have caused the failure of the concrete between the GFRP and the steel. Because this is a numerical simulation, a number of parameters needed to be assumed. In this case, the load was set at 5000 lbs (22 kPa). Ideally, the magnitude of the shear stress should be

71

minimized. In addition, the high shear stress distribution should only be extended over a limited distance, on the order of a few millimeters. Although the interface failure is of concern, it should be noted that the external reinforcement is also less effective with lower shear stresses.

The parameters chosen for the analytical study are as follows:

$E_p =$ Young's modulus of the GFRP;

$G =$ shear modulus of the epoxy;

$f'_c =$ strength of the concrete;

$l_p =$ length of the GFRP;

$t =$ thickness of the GFRP;

$t_1 =$ thickness of the epoxy.

Although only one of these parameters was used in the experimental program, the other parameters are being studied in this analytical model as a seed for future work. With these points in mind, the discussion of the stress distribution follows. Note that further discussion of the stress distribution is purely on the shear stress distribution along the interface between the concrete and the GFRP. The use of the word stress implies shear stress unless noted otherwise.

5.3.1 Stress distribution of the experimental beam

The Matlab program developed in this section is simple. A number of the simplifications and assumptions used in the program develop into some inaccuracies in the results. Figure 5.6 shows the stress distribution along the GFRP as calculated by the analytical model, showing the whole range of stress distribution. Figure 5.7 shows the stress distribution around the location where the load is applied, showing one of the inaccuracies in the model. Another inaccuracy, as mentioned earlier, is the stress distribution at the very end of the composite. Although the stresses in the concrete, steel, and GFRP are all consistent with one another, the simplified model can only show general trends but cannot show significant details.

The first inaccuracy is the sudden jump in the shear stress, as shown by Figure 5.7. This is caused by the idealized loading and moment distribution, as shown in Figure 5.4. The strain distribution in bending, according to beam theory, is dependent upon the bending moment. Although the strain distribution is continuous at the load point, it is not differentiable.

In relating the strains at the soffit of the reinforced concrete beam and the strain within the GFRP, the first derivative of the strain is used. This causes a numerical approximation of the first derivative. This jump in the shear stress is significantly magnified when some of the properties are varied, namely the coefficients to the governing second order differential equation: E_p, G, t_l, t. Although more detailed models can avoid this inaccuracy, the analysis of the results from the model will generally ignore it.

The simple model will show some significant trends, although some inaccuracies exist within the model. These trends can be further explored with more detailed experimental studies and a more sophisticated analytical program to mimic the stress distribution more closely. The trends will be shown and discussed in the following sections.

5.3.2 Changes in material properties: E_p, G, f'_c

In designing the retrofit method for the beam, the GFRP and the epoxy must be chosen. This section shows a variation of a number of factors that may result in decreasing or increasing the stress concentration. In choosing the GFRP and epoxy, special attention should be paid to the elastic properties, in addition to the strength. The effect of the concrete strength, and consequently its Young's modulus, is also studied. The effect of these governing material properties on the shear stress distribution along the interface may be able to allow better prediction the failure mode of the beam.

From the governing second order differential equation, Equation 5.10, it was expected that the Young's modulus of the GFRP, E_p, will play a significant role in the stress distribution. Figure 5.8 shows the stress distributions while E_p is varied. Because the GFRP used in this experiment was much less stiff than expected at 7.16 GPa, it was chosen as the lower bound in this analysis. The Young's modulus was varied as follows: 7.16 GPa (1.04 x 10³ ksi), 50 GPa (7.25 x 10³ ksi), 100 GPa (14.5 x 10³ ksi), 150 GPa (21.8 x 10³ ksi), 200 GPa (29.0 x 10³ ksi). The high end was chosen to be the Young's modulus of steel. It was shown that the stiffer external reinforcement caused consistently higher shear stresses. This may indicate why retrofitting with external steel plates was not always successful due to shear stress transfer problems. With such high shear stresses, the failure of the interface is more likely. This problem has been shown in a number of studies (Meier 1993, Meier et al 1992, Deuring 1993). From Table 2.1, the Young's modulus of the CFRP is significantly higher than that of the GFRP. Meier reported that the most significant problem is the peeling off of the CFRP at

failure. In this case, if the effect of the external reinforcement is to be optimized, then the stiffer materials seem to be more effective in terms of load carrying capacity. However, note that this is done at an increased risk of interfacial bond failure.

Although it was concluded that the stiffer FRP's maybe more effective as external reinforcements, the question lies on the effectiveness of the interface: the epoxy. The shear modulus of the epoxy, G, was varied from 2 GPa to 5 GPa (1.38 x 10^4 to 3.45 x 10^4 ksi). Figure 5.9 shows the results from the analysis. Although the shear stress increases earlier with lower G, the rate of increase in shear stress for stiffer epoxies is much higher. This allows much higher stress concentrations at the end of the GFRP. However, the differences in the ultimate shear stress is not very significant, ranging from about 7 MPa (1.01 ksi) for G = 2 GPa (1.38 x 10^4 ksi) to 12 MPa (1.74 ksi) for G = 5 GPa (3.45 x 10^4 ksi). The higher stress concentration is of significant concern in terms of causing the failure of the concrete between the internal and external reinforcements. From Equation 5.14, we can show that some of the less stiff epoxies can transfer load effectively on to the external reinforcement. This is because the shear stress extends over a longer distance so the epoxies with lower stiffness have much better advantage than very stiff epoxies. Epoxies that are not stiff enough will not be able to transfer the loads on to the GFRP. Variations in the stiffness of the epoxies were experimentally shown by a study by Saadatmanesh and Ehsani (1991). Similar conclusions were also made. Four beams were tested with varying shear stiffnesses of the epoxies. It was observed that the epoxy with very low shear stiffness did not effectively transfer load because the shear stiffness was not high enough to transfer the stress. In contrast, they observed a very brittle delamination failure of the GFRP when the stiff epoxy was used. The analysis shown above confirms these observations.

The concrete strength was also varied. This was done with the purpose of possibly setting guidelines for determining which beams are good candidates for the application of external reinforcements. Figures 5.10 shows effects of the variation of concrete strengths: 3000 psi (20.7 MPa), 5000 psi (34.7 MPa), 8500 psi (58.6 MPa), and 12,000 psi (82.7 MPa). These strengths spanned from low strength to high strength concrete, commonly achieved in large scale construction. The change in concrete strength also changed the elastic modulus of the concrete. The ACI equation for predicting the elastic modulus of the concrete was maintained. From the plot, the analysis showed that the lower strength concrete consistently allowed higher shear forces. This may prove to be a problem because lower compressive strength of concrete also means lower tensile strength. The higher shear stress on the

external reinforcement may likely cause the failure of the concrete between the internal and external tensile reinforcements early on. However, note that some of the differences in the ultimate shear stress are not so significant. The increase in strength from 5000 psi (34.7 MPa) concrete to 12,000 psi (82.7 MPa) concrete only affected a change of 1 MPa (145 psi) in the ultimate shear stress. In contrast, the ultimate shear stress of the 3000 psi (20.7 MPa) concrete was nearly 2 MPa (290 psi) higher than that of the 5000 psi (34.7 MPa) concrete. It maybe concluded that structural elements made of low strength concrete are not good for the use of FRP's as tensile external reinforcements.

From these three analyses, this retrofit method may not be ideal for all types of structures. All three properties affect the shear stress distribution along the interface. Higher stress concentrations at the end of the GFRP carry a higher possibility of failure of the concrete between the GFRP and the steel. However, it can also mean that the external reinforcement is taking higher load. It can be concluded that stiffer external reinforcements maybe more effective in their load carrying capacity and adding stiffness to the section, but they also cause higher shear stress which can cause failure due to the significant stress concentration. The analysis of the stiffness of the epoxy showed that epoxies within a reasonable range of stiffness is best because very stiff epoxies cause too much stress while epoxies without enough stiffness cannot transfer the load effectively. The final conclusion was that low strength concrete is not a good candidate for use with external reinforcements because of the potential for high shear stresses. Along with the high shear stress distribution, the tensile strength of the concrete is also decreased with decreasing compressive strength, increasing the likeliness of the failure of the concrete between the external and internal tensile reinforcements. More detailed experimental and analytical programs are needed to establish reasonable thresholds.

5.3.3 Changes in physical dimensions: length of GFRP, thickness of GFRP, thickness of the epoxy layer

This section looks at the physical parameters. In this case, the length of the GFRP, the thickness of the GFRP, and the thickness of the epoxy layer are the variables. These parameters are potential variables in the design of the retrofit project. The length of the GFRP will play a significant role in both the theoretical design and the cost. The analytical model can also confirm certain failure behavior of the experimental beams. Because the FRP's can come in a variety of thicknesses, this analysis may play a significant role in choosing a more

compatible external reinforcement. Although the thickness of the epoxy cannot be controlled very well in the field, the knowledge of the thickness will allow the stress distribution and possibly failure modes to be better predicted.

First, consider the variation of the length of the GFRP. This variation was seen as the most significant factor in the experimental program. In this case, the following lengths of the GFRP are shown: 24 inches (0.6096 m), 28 inches (0.7112 m), 32 inches (0.8128 m), 36 inches (0.9144 m). Note that the distance between the supports is 36 inches (0.9144 m). Figure 5.11 shows this variation. Two trends can be seen. The stress concentration builds up quickly within the last couple of centimeters to the end of the GFRP. The plot shows what was expected, which is decreasing stress concentration as the GFRP is extended further towards the supports. The differences in the ultimate shear stress are significant. The ultimate shear stress is tripled between the external reinforcements of lengths 24 inches (0.6096 m) and 32 inches (0.8128m). The analysis also showed negligible stress concentration at the end if the external reinforcement is extended all the way to the end of the beam. This behavior was partially confirmed by the experimental program. The failure of the concrete layer between the internal and external reinforcements was dominant failure mode among the failure modes in the beams reinforced with the 28-inch (71-cm) GFRP. However, this failure mode was not so significant with the beams reinforced with the 36-inch (91-cm) GFRP. However, the average failure load of the beams was not consistent with the results of this model. Although the difference in the consistencies of the failure load for the two groups can be explained by the consistencies of the failure mode, the difference in the average cannot be explained in this way. In actual applications, a cost-benefit analysis needs to be done on a case by case basis, considering the risk of this mode of failure and the cost of extending the GFRP further. Note that the external reinforcement may not need to be extended to the supports to avoid this type of failure. They only need to be extended such that the shear stress is within an acceptable range.

Another parameter that can be varied is the thickness of the FRP. FRP's can come in a number of thicknesses, from less than a fifth of a millimeter to a few millimeters thick. In this analysis, the following thicknesses were considered: 0.1 mm (3.94×10^{-3} inch), 0.5 mm (1.97×10^{-2} inch), 1 mm (3.94×10^{-2} inch), 2 mm (7.87×10^{-2} inch). Figure 5.12 shows the results of the analysis. In this case, the thicker FRP behaved similarly to FRP's with higher stiffness, taking on higher loads, as can be seen from the area under the curve. The acceptable thickness of the external reinforcement will likely be dependent upon the shear strength of the

epoxy. In this case, when the material properties of the materials used are established, the thickness can be optimized such that the external reinforcement is effective. At the same time, significant stress concentration can also be avoided.

Finally, consider the changes in the thickness of the epoxy. This, like the changes in the shear strength of the epoxy, will likely play a significant role in the design of the retrofit method. The thicknesses chosen were: 5 mm (0.197 inch), 1 mm (3.94×10^{-2} inch), 0.5 mm (1.96×10^{-2} inch), 0.1 mm (3.94×10^{-3} inch). Figure 5.13 shows the results of the analysis. Again, a similar pattern is shown as with the variation of the shear stiffness of the epoxy. Although the initial stress is higher with thicker epoxy, the stress concentration at the end of the GFRP is much higher for the thinner epoxies. In many cases, as shown by past research presented in the Literature Survey section, the application of the GFRP has been focused on yielding the thinnest layer of epoxy. However, as seen by the results of this model, that may not be the best choice. When the epoxy layer is thicker, the stress transfer from the beam to the external reinforcement takes place over a longer distance. However, it can be optimized to be as effective without causing a significant stress concentration at the end of the external reinforcement. Note that this model is not appropriate for modeling very thick layers of epoxy because it was initially calculated for negligible epoxy thickness, with respect to the beam size. In practice, the thickness of the layer of epoxy and its uniformity may be questionable. Therefore, it may be beneficial to establish guidelines for maximum and minimum thicknesses of the epoxy layer. In practice, after the application of external reinforcements, NDT methods maybe used to find the thickness of the epoxy. Areas where the thickness of the epoxy is outside of the allowable range or voids will need to be redone.

This section has shown possibilities of avoiding significant stress concentrations at the ends of the external reinforcement by varying the length of the FRP, the thickness of the FRP, and the thickness of the epoxy layer. The analysis varying the length of the FRP has confirmed the results from the experiment: the stress concentration at the end of the FRP was higher for shorter FRP sheets. The variation of the thickness of the FRP and the epoxy layer have also shown valuable information for further design and quality control of the application of this method. This model has shown trends that can be confirmed with more detailed models and experimentation.

5.4 Summary

The following is a summary and discussion of the different parameters varied in the analytical model. The model showed some significant trends that can be further explored in future experimental and analytical work.

Concrete strength (f'_c)

- The variation in concrete strength was done to explore the possibility of setting guidelines for whether or not a structural member is a good candidate for the application of external reinforcements. The concrete strength was varied from low strength concrete to commercially available high strength concrete: 3000 psi (20.7 MPa), 5000 psi (34.7 MPa), 8500 psi (58.6 MPa), and 12,000 psi (82.7 MPa).

- The result showed that low strength concrete was not a good candidate for this type of strengthening method because the stress concentration was significantly higher. Coupled with lower strength, the possibility of premature failure of the retrofit method is high.

Thickness and Young's modulus of the GFRP

- The thickness and the Young's modulus of the FRP are related. As they increase, the stiffness of the FRP sheets increase. Both of these variables can be specified when the material is ordered so there is control over this parameter.

- Both of these parameters showed similar trends. As the stiffness or thickness of the FRP increase, the shear stress concentration increases significantly. The increase in the stress concentration seems to decrease with successive increases in the thickness or the stiffness of the GFRP. For example, the most significant increase for the Young's modulus was between 7.16 GPa (1.03×10^3 ksi) and 50 GPa (7.25×10^3 ksi), which the stress concentration jumped from 7 MPa (1.0 ksi) to 16 MPa (2.3 ksi). In contrast, the increase of the Young's modulus from 50 GPa (7.25×10^3 ksi) to 200 GPa (29×10^3 ksi) only increased the stress concentration from 16 MPa (2.3 ksi) to 20 MPa (2.9 ksi). By working with both the thickness and the Young's modulus of the GFRP, the stress concentration can be controlled.

Shear modulus and thickness of the epoxy

- Recall Equation 5.3 where the shear stress is proportional to the ratio of the shear modulus to the thickness of the epoxy. These parameters were varied to study whether or not they can be optimized to control the stress concentration. However, that needs to be done without significant scarifice to the effectiveness of the stress transfer.

- The results from the model showed that both the shear modulus and the thickness of the epoxy can be optimized. The stress can still be effectively transferred between the reinforced concrete beam and the GFRP sheet while the stress concentration at the end of the GFRP is controlled within reasonable range. For example, very high shear modulus or very thin layer of epoxy may cause a significant stress concentration. However, since the decrease in the shear modulus or the increase in the thickness also causes an earlier increase in the shear stress, although at a lower rate, a similar effectiveness in the stress transfer can be achieved.

Length of the GFRP

- The variation in the length of the GFRP was the primary reason for formulating this analytical model. It was observed that a dominant failure mode in the beams retrofitted with the 28-inch (71-cm) GFRP was the failure of the concrete layer between the internal and external reinforcements. This mode of failure is likely due to the stress concentration at the end of the GFRP.

- The significantly higher stress concentration at the end of the GFRP for the shorter external reinforcements was confirmed by the analytical model. From the analytical model, the stress concentration for the beams with the GFRP extending the full length of the span was negligible, at least two orders of magnitude less than that of the 24-in (61-cm). In contrast, the shear stress concentration can be as high as 13 MPa (1.88 ksi) when the GFRP was 24 inches (61 cm) long. Although the results of the analytical model was consistent with the failure mode observed, the differences in the average failure load between the beams reinforced with 28-inch (71-cm) and 36-inch (91-cm) GFRP remain unexplained.
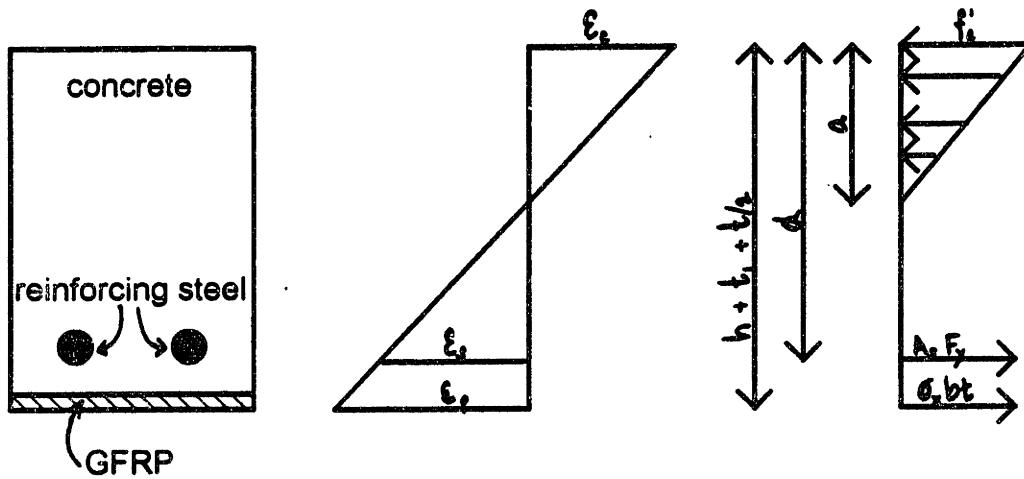
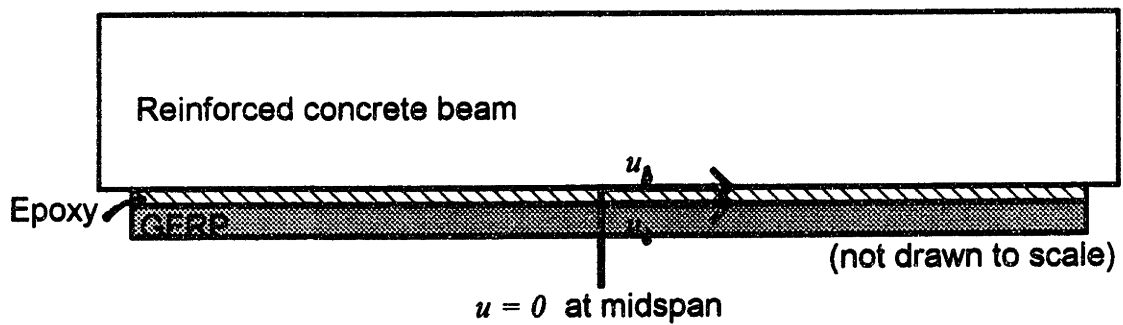Figure 5.1 Assumed stress and strain distribution on the retrofitted section

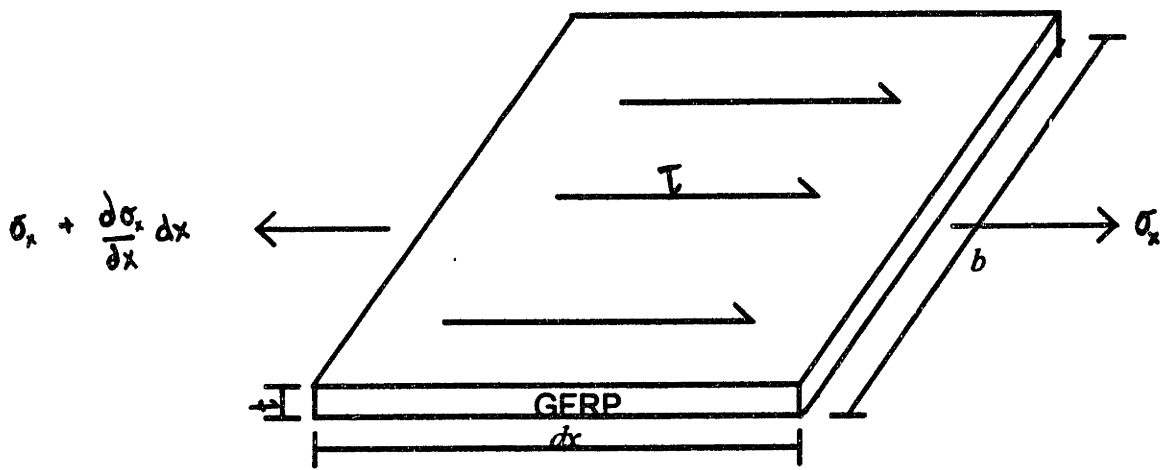Figure 5.2 Orientation of the nomenclature

Figure 5.3 Shear stress distribution and equilibrium diagram for
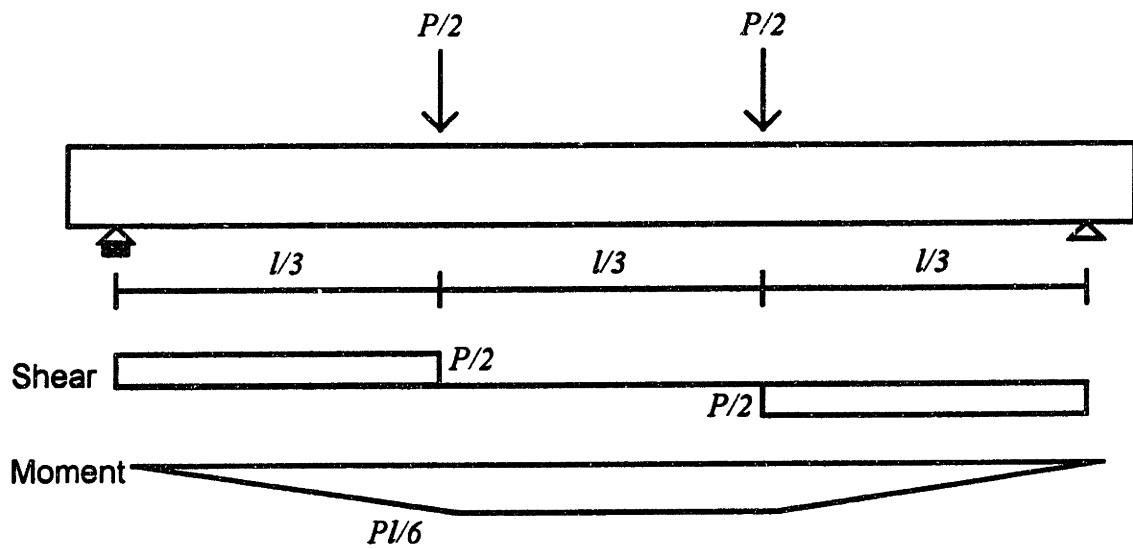an elemental piece of the GFRP

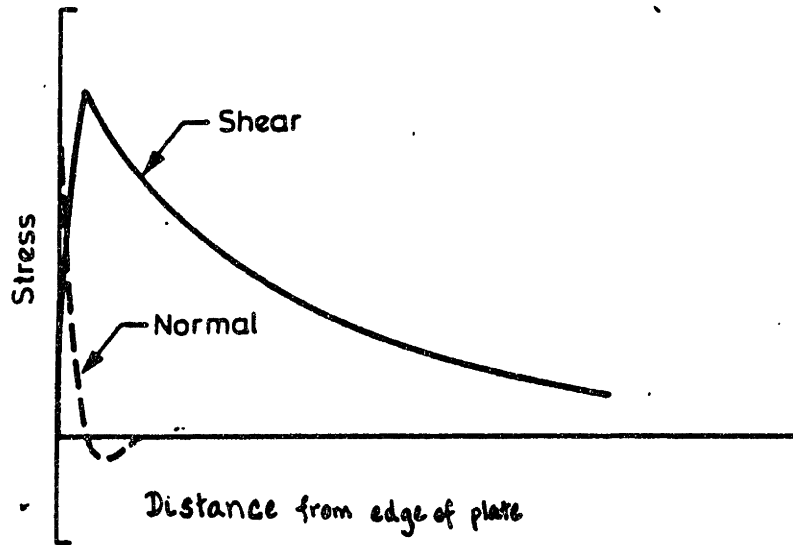Figure 5.4 Shear and moment distribution due to external loads

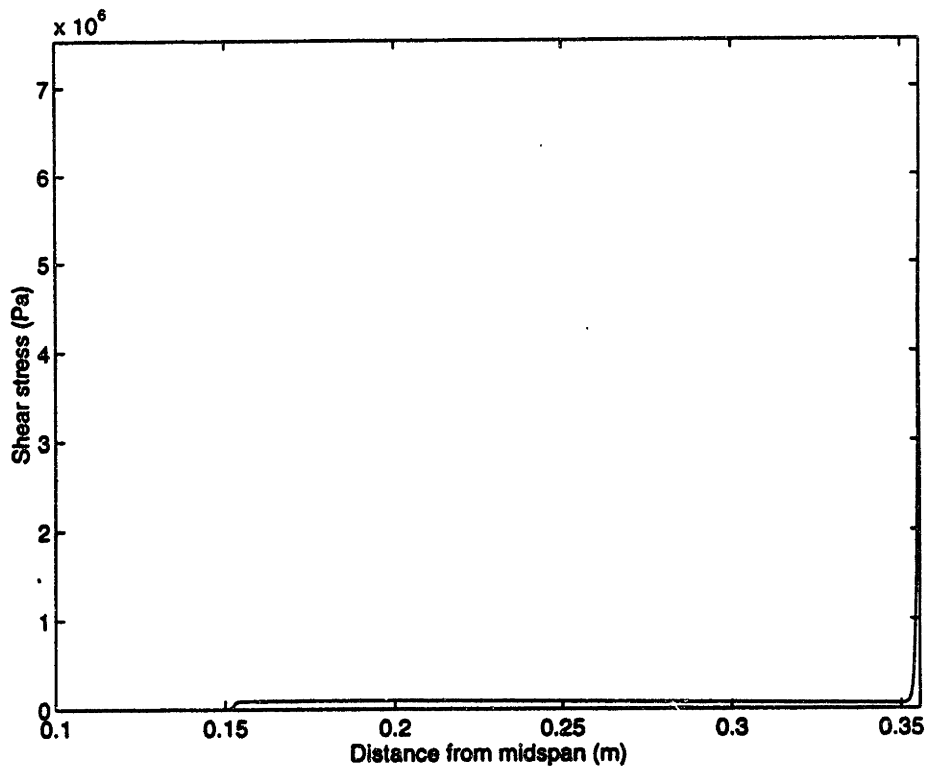Figure 5.5 Actual stress distribution (Roberts 1989)

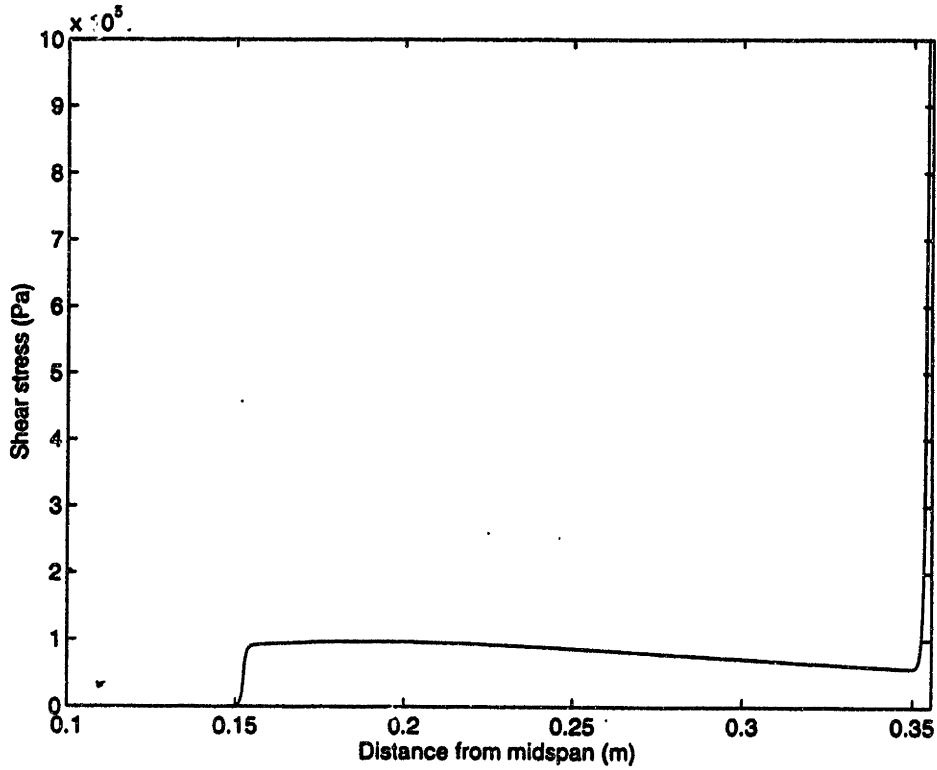Figure 5.6 Stress distribution of the experimental beam

Figure 5.7 More focused view of a section of the plot presented in Figure 5.6
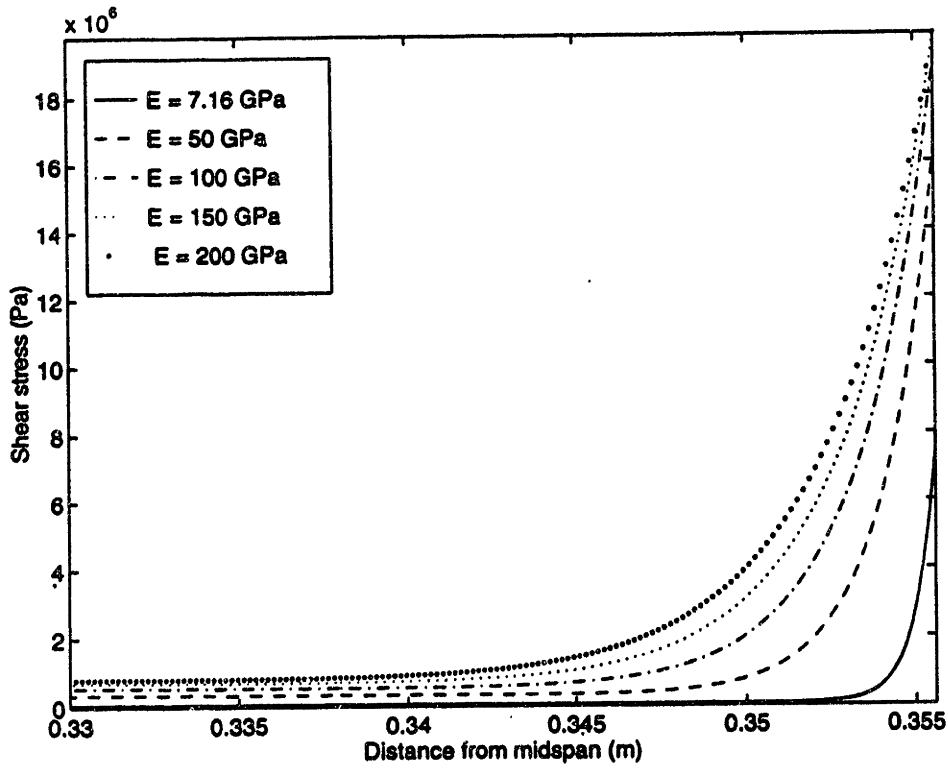

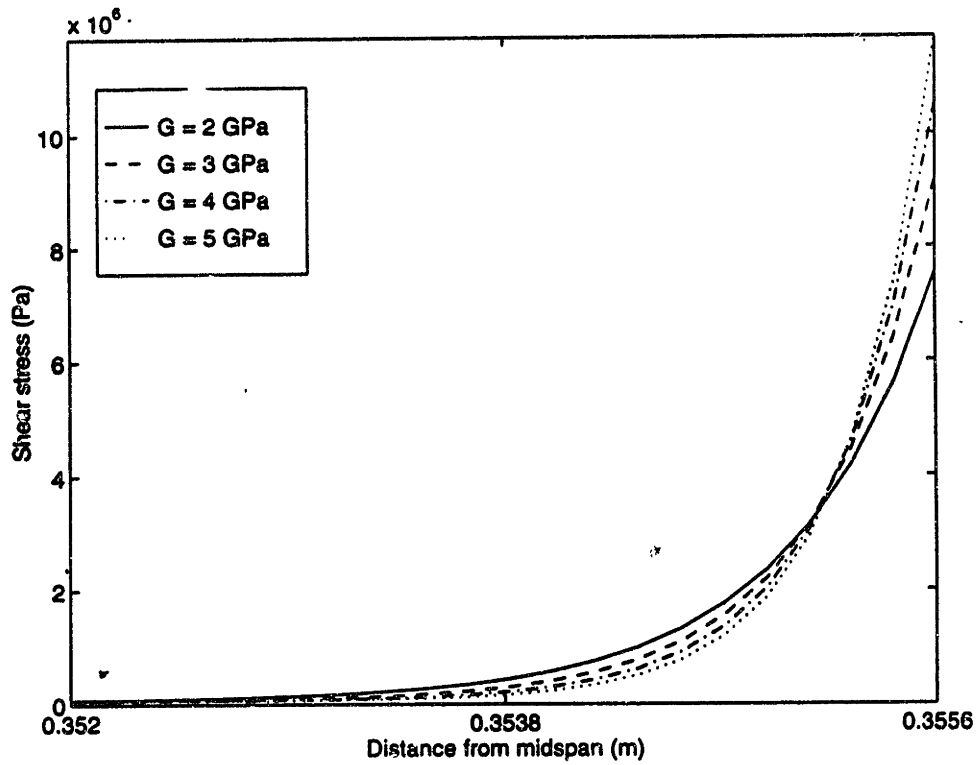Figure 5.8 Stress distribution varying the Young's modulus of the FRP

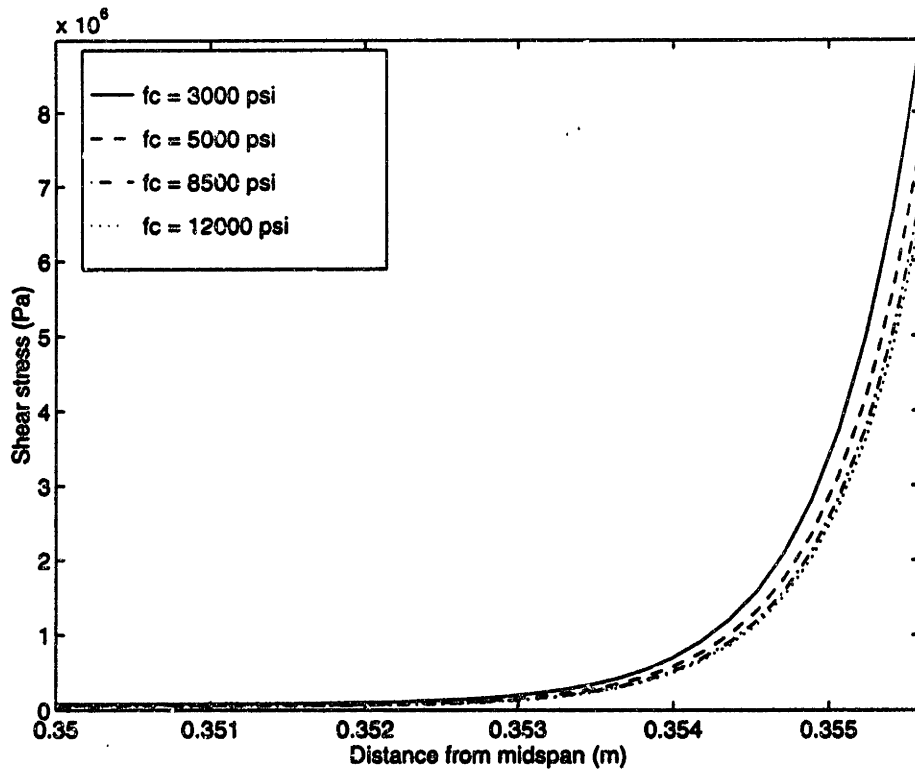Figure 5.9 Stress distribution varying the shear modulus of the epoxy

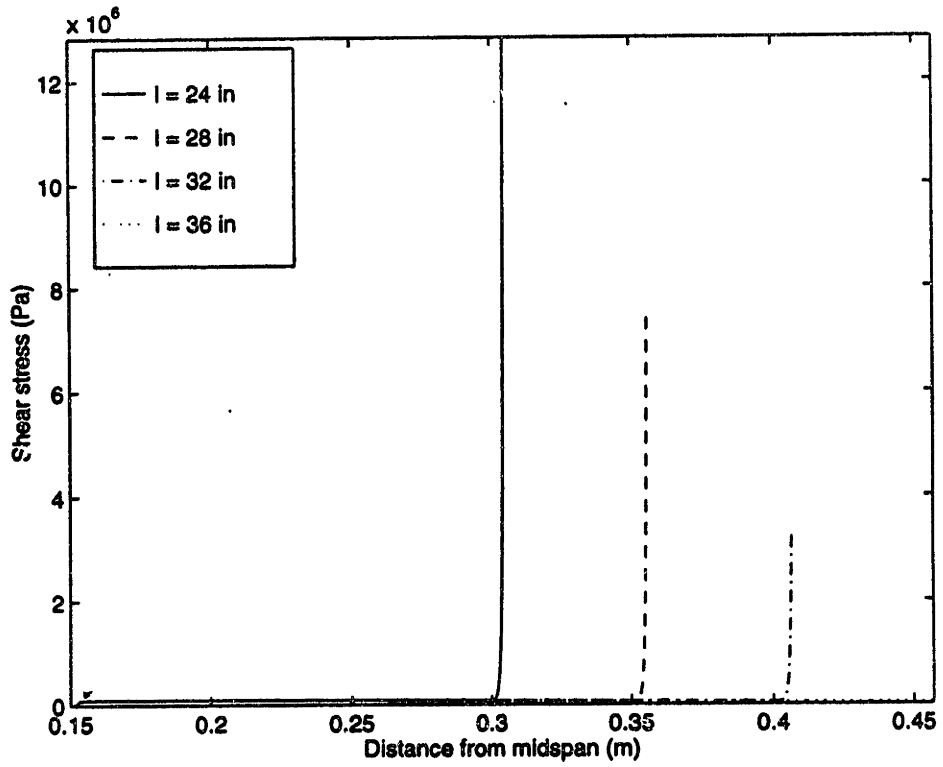Figure 5.10 Stress distribution varying the concrete strength

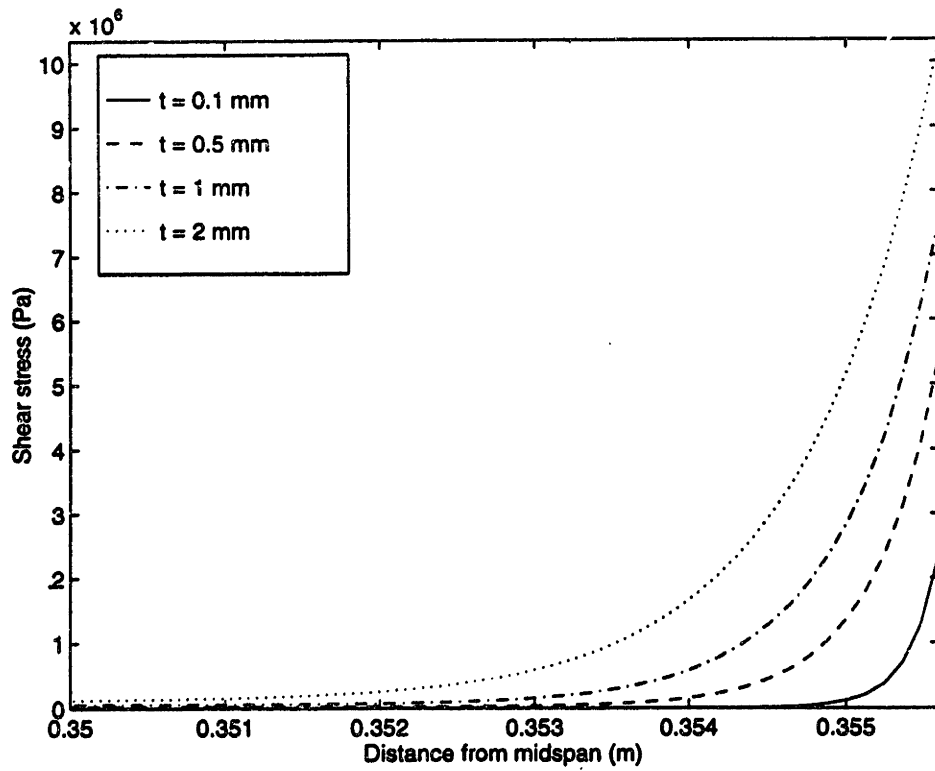Figure 5.11 Stress distribution varying the length of the external reinforcement

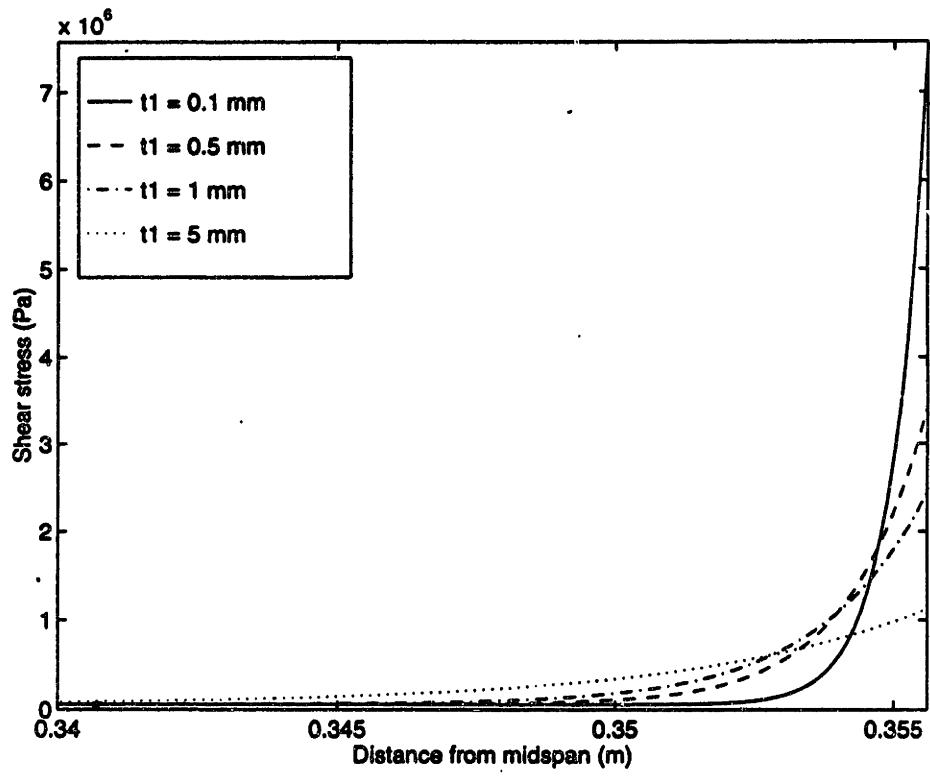Figure 5.12 Stress distribution varying the thickness of the composite

Figure 5.13 Stress distribution varying the thickness of the epoxy

6 Summary, conclusions, and recommendations for future work

6.1 Summary

The use of GFRP's as external reinforcements has been shown to increase the flexural strength of reinforced concrete beam. However, the failure behavior is not yet understood thoroughly. Unlike the behavior of reinforced concrete beams, the retrofitted beams have a tendency to fail in a number of failure modes, for example, shear failure, concrete crushing, and the failure of the concrete between the internal and external reinforcements. Many of these failure modes are distinctly different from the failure modes of traditionally reinforced concrete beams. The more frequent shear failure stems from retrofitting the beams in flexure and not in shear so the increased flexural strength approaches the design shear strength. This project was designed to study the shear behavior of pre-loaded, steel reinforced concrete beam retrofitted with epoxy bonded GFRP sheet on the tension side of the beam. Both experimental and analytical programs were carried out to study the failure behavior and their possible causes.

6.1.1 Description of experimental and analytical programs

In the experimental program, traditionally reinforced concrete beams were design and cast. The beams were 3 inches x 5 inches x 42 inches (7.6 cm x 13 cm x 107 cm). Type III cement was used for high early strength concrete. The beams were reinforced with two #3 50-ksi (345-GPa) bars. A 4-point loading scheme was used in the experiment. The testing machine allowed 36 inches (91 cm) unsupported span and the beam was loaded at 12 inches (30 cm) from the support. These beams were pre-loaded to introduce shear and flexural cracks. Then, the GFRP sheet was applied, and the beam was tested until failure. The variables in the experimental program were shear strength (by varying stirrup spacing), surface texture of the GFRP, and the length of the GFRP. Along with controlled beams, there were 10 combinations. Three identical beams of each designation were cast. The results of 30 beams were presented in this report.

The analytical program was developed as a direct extension of the experimental program. The experimental values of the material properties and dimensions were used in formulating the analytical model. The model was a one-dimensional model of the shear stress distribution along the interface between the concrete and the GFRP. In formulating the model, a few simplifying assumptions were made. Both the GFRP and the steel were assumed to behave in a linear elastic manner. Under a load of 5000 lbs (22 kN), the stress was checked to be within the acceptable range. This load was used for analytical purposes. The tensile strength of the concrete is assumed negligible. In this model, the shear strength of the reinforced concrete beam does not play a role. In addition, the surface texture of the GFRP could not be quantified and used as a parameter in this model. Therefore, the variables in this model are the length of the GFRP, the thickness of the GFRP, the Young's modulus of the GFRP, the thickness of the epoxy, the shear modulus of the epoxy, and the concrete strength.

6.1.2 Results of the experimental and analytical programs

Two of the experimental variables did not show much significance: the variation in the stirrup spacings and the different surface textures of the GFRP sheet. The effects of the difference in two stirrup spacings were not apparent in the experimental results. The rough and smooth surface texture of the GFRP was also overwhelmed by other experimental parameters that the experimental results from the two groups were not distinguishable. The most apparent experimental variable was the length of the GFRP. The strength of the beams retrofitted with the 28-inch (71-cm) long GFRP sheet was significantly higher than those retrofitted with the 36-inch (91-cm) long GFRP sheet, which were higher than the beams that were not retrofitted at all. Six types of failure modes were observed in the failure of the retrofitted beams. All of them were observed among the beams retrofitted with the 36-inch (91-cm) long GFRP. In contrast, the beams retrofitted with the 28-inch (71-cm) long GFRP sheet consistently failed due to the failure of the layer of concrete between the internal and external reinforcements. Five out of 16 beams failed in this manner in contrast to only two beams retrofitted with 36-inch (91-cm) long GFRP. This particular type of failure indicates the high shear stress concentration at the end of the external reinforcement. However, since the bond along the interface between the concrete and the GFRP was strong enough, the failure was shifted to the concrete layer adjacent to the interface. The stress concentration at the end of the GFRP is further studied in the analytical program to better understand the important parameters involved.

As mentioned earlier, the failure of the concrete layer between the internal and external reinforcements indicated sufficient bond was established between the concrete and GFRP. This shifted the failure from the interface to the concrete layer. The results of the analytical program confirmed that the shorter external reinforcements cause much higher shear stress concentrations on the concrete beam. In addition, low strength concrete was shown to be unacceptable for the application of external reinforcements because it resulted in high shear stresses, which magnifies the problem when coupled with the lower strength concrete. The thickness and the Young's modulus of the GFRP are directly related to the stiffness, and the model showed that higher stress concentrations occurred with stiffer GFRP sheets. However, note that higher stress concentrations can also mean that the GFRP is working more efficiently. In contrast, the analysis showed that the thickness and shear modulus of the epoxy can be optimized. When the stiffness is too high or the thickness is too low, the stress concentration is very high. However, when the reverse is true, the GFRP may not be effective as an external reinforcement. Given other parameters, the properties of the epoxy can be optimized such that the stress concentration is limited. Further experimental work is needed to confirm these analytical results.

The results of the experimental program indicated that the shear stress concentration at the ends of the GFRP maybe a primary cause of failure for a few experimental beams. This problem has been addressed by a number of other research groups (Ritchie et al 1991, Saadatmanesh and Ehsani 1990, Saadatmanesh and Ehsani 1991, Sharif et al 1991). Because the length parameter was the only significant experimental parameter, the analytical program confirmed those experimental results and further explored other parameters that can be explored in future research.

6.2 Conclusions

Although the use of GFRP as external reinforcements for reinforced concrete beams has been shown to be a promising repair and strengthening technique, the behavior of the retrofitted beams is still not well understood, especially when shear failure is involved. Without this understanding, the failure mode and, consequently, the strength of the retrofitted beams cannot be predicted. The widespread application of the use of GFRP's as external reinforcement cannot be achieved unless the method can be efficiently and accurately designed. The experimental program suggested a number of failure modes, some of which have been suggested by past research. The analytical program, although relatively simple in form, allowed

preliminary exploration of a number of parameters affecting the transfer of forces at the interface between the concrete and the GFRP. Together, the experimental and analytical programs, pointed to important parameters affecting the shear transfer between the concrete and the GFRP. Further experimental and analytical work are still needed to confirm these trends before design guidelines can be fully developed.

6.3 Recommendations for future work

Based on the results of this study, the following are recommendations for future work:

- Both the experimental and analytical results showed that the length of the external reinforcement is an important parameter. The variation in the length can cause significant shifts in failure modes. With better understanding of the behavior of the retrofitted beam with respect to the length of the external reinforcement, the method can also be safer, more cost effective, and more attractive for widespread use.

- Strengthening of the reinforced concrete beam should consider both flexural and shear strength. If the beams are retrofitted in flexure, the upper limit for this retrofit method is the design shear strength. However, this upper limit should not be approached because the shear behavior is still not well understood. The shear behavior should be avoided as with the design of traditionally reinforced concrete beams.

- The analytical program explored a number of parameters that may affect the shear stress distribution along the interface between the concrete and GFRP. Further exploration should focus on these parameters: concrete strength, length of the GFRP, thickness of the GFRP, Young's modulus of the GFRP, thickness of the epoxy, and the shear modulus of the epoxy.

- Anchorage and other ways for limiting the stress concentration at the ends of the external reinforcement should be explored.

- The simple model used in this project proved to be a useful tool for preliminary work. More detailed analysis, like the use of finite elements analysis, should not be used for exploratory work.

- The experimental parameters that are not variables should be controlled as much as possible, e.g. mixing few large batches of concrete instead of many smaller batches to avoid the effects of concrete strength rising as an uncontrolled variable.

- Larger models and full-scale tests should be conducted on practical methods for applying external reinforcements to ensure good interface bond.

Bibliography

Arduni, M., A. D'Ambrisi, and A. Di Tomasso. (1994) "Shear failure of concrete beams reinforced with FRP plates" Infrastructure: New materials and methods of repair (Proceedings from the Third Materials Engineering Conference). New York: American Society of Civil Engineer, pp. 123-131.

Ashby, M. F. and D. R. H. Jones. (1980) Engineering materials I. Oxford, England: Pergammon Press.

Billington, D. P. (1983) The tower and the bridge: The new art of structural engineering. Princeton, New Jersey: Princeton University Press.

Chajes, M. J. (1996) Department of Civil and Environmental Engineering, University of Delaware, 28 October 1996. Interview with author, University of Delaware.

Chajes, M. J., T. A. Thomson, Jr., C. A. Farschman. (1995) "Durability of concrete beams externally reinforced with composite fabrics," Construction and building materials. Vol. 9, No. 3, 141-148.

Chajes, M. J., T. A. Thomson, Jr., T. F. Januszka, W. W. Finch, Jr. (1994) "Flexural strengthening of concrete beams using externally bonded composite materials," Construction and building materials. Vol. 8, No. 3, 191-200.

Cooper, J. D. (1991) Advanced composites - Backbone for a new era in bridge engineering research. Keynote speaker ASCE Specialty Conference on Advanced Conference in Civil Engineering Structures, Las Vegas, January 31 and February 1, 1991.

Deuring, M. (1993) Verstarken von Stahlbeton mit gespannten Faserverbund-Werkstoffen. Switzerland: EMPA film.

Devore, J. L. Probability and statistics for engineering and the sciences, Third edition. Pacific grove, CA: Brooks/Cole Publishing Company, 1991.

Dussek, I. J. (1980) "Strengthening of bridge beams and similar structures by means of epoxy-resin-bonded external reinforcement," Transportation research record 785. 21-24.

Finch, W. W., Jr., M. J. Chajes, D. R. Mertz, V. N. Kaliakin, A. Faqiri. (1994) "Bridge rehabilitation using composite materials," Infrastructure: New materials and methods of repair (Proceedings from the Third Materials Engineering Conference). New York: American Society of Civil Engineer, 1140-1147.

Herb Celanese, Inc. (1996) "Material specifications for Celanese Nylon Glass Fiber Reinforced Plastic Grade 1600 with 30% glass fibers." Brochure from Herb Celanese, Inc., NJ.

McCormick, F. C. (1985) Field study of a pedestrian bridge of reinforced plastics. Virginia Highway and Transportation Research Council, Final report, May 1976 to September 1985, VHTRC86-R21, December 1985, TRIS 453676.

Meier, U. (1991) Ibach Brucke. Switzerland: EMPA film.

Meier, U. (1993) "Carbon fiber-reinforced polymers: Modern materials in bridge engineering," Structural engineering International. November: 7-12.

Meier, U., M. Deuring, H. Meier, G. Schwegler. (1992) "Strengthening of structures with CFRP laminates: Research and applications in Switzerland," Advanced composite materials in bridges and structures. Canada: Canadian Society of Civil Engineering.

Nilson, A. H. and G. Winter. (1991) Design of concrete structures. New York: McGraw-Hill.

Ritchie, P. A., D. A. Thomas, L. Lu, G. M. Conelly. (1991) "External reinforcement of concrete beams using fiber reinforced plastics," ACI structural journal. July-August: 490-500.

Roberts, T. M. (1989) "Approximate analysis of the shear and normal stress concentrations in the adhesive layer of plated RC beams," The structural engineer. June, 229-233.

Roberts, T. M., H. Haji-Kazemi. (1989) "Theoretical study of the behavior of reinforced concrete beams strengthened by externall bonded steel plates," Proceedings of the institution of civil engineers. London, England: Thomas Telford, 39-55.

Saadatmanesh, H., M. R. Ehsani. (1990) "Fiber composite plates can strengthen beam," Concrete international. March: 65-71.

Saadatmanesh, H., M. R. Ehsani. (1991) "RC beams strengthened with GFRP plates I: Experimental study," Journal of structural engineering. November: 3417-3433.

Schwegler, G. (1994) Mit Faserverbundwerkstoffen verstarktes Mauerwerk in seismisch gefahrdeten Zonen. Switzerland: EMPA film.

Sharif, A., G. J. Al-Sulaimani, I. A. Basunbul, M. H. Baluch, B. N. Ghaleb. (1991) "Strengthening of initially loaded reinforced concrete beams using FRP plates," ACI Structural Journal. March-April: 160-168.

Shu, Y. (1983) "Chinese crossing first for plastic pioneers," New civil engineer. 14 April.

Sierakowski, R. L., C. A. Ross, J. W., Tedesco, M. L. Hughes. (1994) "Concrete beams with externally bonded carbon fiber reinforced plastic (CFRP) strips," Infrastructure: New materials and methods of repair (Proceedings from the Third Materials Engineering Conference). New York: American Society of Civil Engineer, 139-146.

Sika Corporation. (1996) "Material specifications for Sikadur 31: high-modulus, high-strength, structural, epoxy paste adhesive." Brochure from Sika Corporation, Lynndhurst, NJ.

Tonen Corporation. (1996) Tonen Forca Tow Sheet: Carbon fiber sheet strengthening of concrete and masonry. Brochure from the Tonen Corportation.

Triantafillou, T. C., N. Deskovic, M. Deuring. (1992) "Strengthening of concrete structures with prestressed fiber reinforced plastic sheets," ACI Structural journal. May-June: 235-244.

Xanthakos, P. P. (1996) Bridge strengthening and rehabilitation. Upper Saddle River, NJ: Prentice Hall.

Ziraba, Y. N., M. H. Baluch, I. A. Basunbul, A. M. Sharif, A. K. Azad, G. J. Al-Sulaimani. (1994) "Guidelines toward the design of reinforced concrete beams with external plates," ACI structural journal. November-December: 639-646.

Appendix A Matlab script file: bmn.m

The following Matlab script file uses the finite difference method and LU decomposition to solve the second order differential equation presented in Equation 5.10. The rest of the program follows the reasoning of the constitutive relations given in section 5.2.2. The equation numbers presented in italics refer to the equations used in the text of the report.

```
% Wilasa Vichit-Vadakan
% Start date: November 29, 1996
% End date: December 6, 1996


% Finite difference method for solving a second order differential equation
% system.  The LU decomposition assumes a banded tridiagonal system.


% Constants and variables used:
%
% Es = Young's modulus of steel         b = width of beam
% Ec = Young's modulus of concrete      h = height of beam
% Ep = Young's modulus of the frp       d = distance from the top of the beam to the steel
% G = Shear modulus of the plastic      t = thickness of the frp
% fc = concrete strength                t1 = thickness of the epoxy
%                                       l = length of beam
%                                       As = area of steel
%                                       a = effective height of concrete in compression
% ub = x-displacement of the beam
% up = x-displacement of the frp
% taob = shear stress in concrete
% sigmap = stress in plastic

clear;

        % Defining the constants.
fc = 3.4475e7;
Ec = 57000*((fc/6895)^0.5)*6895;
Ep = 7.160e9;
G = 1.989e9;
t=1e-3;
t1=1e-4;
Es = 1.9996e11;
fs=3.4475e8;
b=7.62e-2;
h = 1.27e-1;
d=8.89e-2;
As=1.42e-4;
I=4.91e-6;
a=2.35e-2;
lb = 9.144e-1;
elements = 2000;
```

```
P = 4448*5;
NA = a;

        % Limits of calculation
upper = 0.3556;
lower = 0;
stopiterations = 5;

        % Calculating element size
dx = (upper-lower)./(elements);

        % Calculating ub.
x = lower:dx:upper;
[width length] = size(x);
M = (P*lb/6)*(1-(x-lb/6)/(lb/3));
loadpoint = round (lb/(6*dx));
for count =1:loadpoint
    M(count) = P*lb/6;
  end;
integral = 0;
uB(1) = 0;
inside = M.*(h-NA)./(Ec*I);
for count = 2:length
    integral = integral + dx.*0.5*(inside(count-1) + inside(count));
    uB(count) = integral;
  end;
uB = abs(uB);
%plot (x,uB);
%xlabel ('Distance from midspan (m)');
%ylabel ('Displacement in beam (m)');
%title ('Displacement in beam with respect to the distance from midspan')

for iterations = 1:stopiterations

        % LU decomposition to calculate uc from given uB
[width length] = size(x);
A = Ep * t * t1 / G;
for count = 1:(length)
    e(count) = A./(dx*dx);
    f(count) = -2*A./(dx*dx)-1;
    g(count) = A./(dx*dx);
  end;
e(1) = 0;
e(length) = 2*e(length);
r = -uB(iterations,:);
for count = 2:(length)
    e(count) = e(count) / f(count -1);
    f(count) = f(count) - e(count) * g(count -1);
  end;
```

Equation 5.11

95

```
for count = 2:(length)
    r(count) = r(count) - e(count) * r(count-1);
    end;
uc(iterations, length) = r(length)/f(length);
for count = (length-1):-1:2
    uc(iterations, count) = (r(count) - g(count).*uc(iterations, count+1))./f(count);
    end;
uc(iterations,1) = 0;


        % Calculating shear stress
tao(iterations, :) = G.*(uB(iterations, :)-uc(iterations, :))./t1;
tao(iterations, :) = abs(tao(iterations, :));
%plot (x,tao(interations, :));
%xlabel ('Distance from midspan (m)');
%ylabel ('Shear stress (Pa)')
%Title ('Shear stress distribution along the length of the plastic');


        % Calculating stress in plastic

[width length] = size (x);
forcep(iterations, length) = 0;
integral = dx*(tao(iterations, length)+tao(iterations, length-1))/2;
forcep (iterations, length) = 0;
for count = (length-1):-1:2
    integral = integral + dx*(tao(iterations, count)+tao(iterations, count-1))/2;
    forcep(iterations, count) = integral*t;
    end;
forcep (iterations, 1) = forcep (iterations, 2);
forcep(iterations,:) = abs(forcep(iterations,:));
%plot (x, forcep);
%xlabel ('Distance from midspan (m)');
%ylabel ('Force exerted by the plastic (N)')
%Title ('Force distribution along the length of the plastic');
%hold on;


        % Redistributing forces

q=-fc*b/6;
r=0.5*fc*b*d;
s=forcep(iterations,:)*(d-h)-M;
inside = r*r-4*q.*s;
a=(-r+sqrt(inside))./(2*q);
fs = (fc.*a.*b-forcep(iterations,:))./As;
ns = Es/Ec;
np = Ep/Ec;
if iterations < 2
    I = x-x;
    end;
I(iterations,:) =b*a.*a.*a./3+ns*As.*(d-a).*(d-a)+np*b*t.*(h-a).*(h-a);
```

Equation 5.3

Equation 5.12

96

```
MRC = M - forcep(iterations,:).*(h+t/2-a);                    Equation 5.15
integral = 0;
uB(iterations+1, 1) = 0;
inside = MRC.*(h-NA)./(Ec*I(iterations, :));
for count = 2:length
    integral = integral + dx*0.5*(inside(count-1) + inside(count));
    uB(iterations+1, count) = integral;
  end;
uB(iterations+1,:) = abs (uB(iterations+1,:));
%plot (x,uBnew,'b');
%xlabel ('Distance from midspan (m)');
%ylabel ('Displacement in beam (m)');
%title ('Displacement in beam with respect to the distance from midspan')

end;

shear = tao(stopiterations,:);
sigmap = (forcep(stopiterations,:))./(b*t);
plot (x, shear);
```

k

Appendix B Matlab script file: vary.m

This Matlab script file uses the other matlab script file, bmn.m, to calculate the stress distribution. This file allows variations in the material properties and compiles the final stress distribution.

```
% Wilasa Vichit-Vadakan
% Start date: November 16, 1996
% End date: November 19, 1996


% This program uses the script file bmn.m to calculate the shear
% stress distribution while different properties are varied.

hold off;

        % Variation 1

clear;
Ep = 3.41e9;
fc = 3.4475e7;
G = 1.989e9;
upper = 0.3556;
t = 1e-3;
t1 = 5e-3;
Ec = 6895*57000*(fc/6895)^0.5;
beamsh;
plot (x, shear);
hold on;

        % Variation 2

clear;
Ep = 3.41e9;
fc = 3.4475e7;
G = 1.989e9;
upper = 0.3556;
t = 1e-3;
t1 = 1e-3;
Ec = 10^3*6.895*57000*(fc/(6.895*10^3))^0.5;
beamsh;
plot (x, shear,'g--');

        % Variation 3

clear;
Ep = 3.41e9;
fc = 3.4475e7;
G = 1.989e9;
upper = 0.3556;
```

```
t = 1e-3;
t1 = 5e-4;
Ec = 10^3*6.895*57000*(fc/(6.895*10^3))^0.5;
beamsh;
plot (x, shear,'m-.');
```

% Variation 4

```
clear;
Ep = 3.41e9;
fc = 3.4475e7;
G = 1.989e9;
upper = 0.3556;
t = 1e-3;
t1 = 1e-4;
Ec = 10^3*6.895*57000*(fc/(6.895*10^3))^0.5;
beamsh;
plot (x, shear, 'b:');

xlabel ('Distance from midspan (m)');
ylabel ('Shear stress (Pa)')
legend ('Variation 1','Variation 2','Variation 3','Variation 4');
```

THESIS PROCESSING SLIP

FIXED FIELD: ill _____ name _____

index _____ biblio _____

▶ COPIES: (Archives)   Aero   Dewey   (Eng)   Hum

Lindgren   Music   Rotch   Science

TITLE VARIES: ▶☐ _____

_____

_____

NAME VARIES: ▶☐ _____

_____

IMPRINT   (COPYRIGHT) _____

▶ COLLATION: ___99ℓ_____

_____

▶ ADD. DEGREE: _____ ▶ DEPT.: _____

SUPERVISORS: _____

_____

___ __ _____

___ __ _____

___ __ _____

___ __ _____

___ __ _____

___ __ _____

NOTES:

cat'r: _____   date: _____

page: ▶ F38

▶ DEPT: __C.E._____

▶ YEAR: __1997_____ ▶ DEGREE: __M.S.__

▶ NAME: __VICHIT-VADAKAN, Wilasa__